Distribution, Sources, and Dynamics of Particulate Matter Along Trans-Arctic Sections

Wilford D. Gardner

Department of Oceanography, Texas A&M University, College Station, TX 77843 USA

ORCID # 0000-0002-6299-3744

Mary Jo Richardson

Department of Oceanography, Texas A&M University, College Station, TX 77843 USA

ORCID # 0000-0001-9583-139X

Alexey V. Mishonov

CISESS/ESSIC/University of Maryland, NCEI/NOAA affiliate, Silver Spring, MD, USA

ORCID # 0000-0002-2958-8747

Phoebe J. Lam

Department of Ocean Sciences, University of California, Santa Cruz, CA 95064 USA

ORCID # 0000-0001-6609-698X

Yang Xiang

Department of Ocean Sciences, University of California, Santa Cruz, CA 95064 USA

ORCID # 0000-0003-1862-0948

*Corresponding author: Wilford D. Gardner: wgardner@ocean.tamu.edu, P: 1-979-845-3928

Texas A&M University, College Station, TX 77843. ORCID # 0000-0002-6299-3744

3 Key points:

1. First trans-Arctic section of beam attenuation (Cp) and Chl-*a* concentrations reveals significant interaction with trans-Arctic hydrography.

2. Optical proxies for particle mass, particular organic carbon, and Chl-a enable general identification of particle sources and dynamics.

3. Intermediate and bottom nepheloid layers based on Cp and Aluminum provide evidence of sediment transport from margins to basins.

Abstract

In order to better understand the sources, sinks and hydrodynamic/biogeochemical influences on particulate matter distribution and variability in Arctic basins, we combined data from two 2015 fall expeditions: one from Bering Strait (USCGC Healy) and the other from Barents Sea (R/V Polarstern) meeting at the North Pole. Sections of beam attenuation due to particles were overlain by salinity, temperature, and chlorophyll-*a* fluorescence (Chl-*a*), and with nitrate contours on Chl-*a* sections to compare with concentrations of particulate matter (PM) and particulate organic carbon (POC) from full water column filtered samples. Dense Pacific water moving swiftly through Bering Strait erodes and carries sediment-laden waters onto the Chukchi Shelf, much of it moving in and above Barrow Canyon or is entrained in eddies. This nutrient-rich Pacific water sinks below the low-salinity, nutrient-poor polar mixed layer, forming a thick lens of high salinity water known as Pacific halocline waters. The nutrient-poor mixed layer inhibits photosynthesis in surface waters of Canada and Makarov Basins, but subsurface Chl-*a* maxima are observed when nutrients are available. Surface-water POC biomass appears greater in Barents Sea than in Beaufort Sea because nutrient-rich Atlantic water entering Barents Sea is not isolated from surface waters by strong stratification. Surface water freezes, creating high-density water that cascades into 400 m basins in Barents Sea and into deep Nansen Basin, eroding sediment that forms patches of nepheloid layers in the shallow basins. Nepheloid layers in the deep basins are very weak, consistent with a lack of strong currents there.

Plain Language Summary

In order to better understand the sources, sinks and hydrodynamic/biogeochemical influences on particulate matter distribution in the Arctic basin, we combined data from two 2015 fall expeditions: one aboard USCGC Healy (USA) going from Bering Strait and the other aboard R/V Polarstern (Germany) from Norway, and meeting at the North Pole. Optical measurements of particle concentration throughout the water column were coupled with simultaneous measurements of salinity, temperature, Chl-*a* fluorescence, and nitrate. Particle composition analyzed from filtered samples aided significantly in discerning sources, distribution and dynamics of particles. Dense, nutrient-rich Pacific water comes through Bering Strait and sinks below a thin, low-density, low-nutrient surface mixed layer, forming a thick lens of high salinity water. The nutrient-poor mixed layer inhibits surface-water photosynthesis in Canada and Makarov Basins, but subsurface Chl-*a* maxima are observed when nutrients are available. Nutrient-rich Atlantic water enters the Barents Sea. Surface water freezes, creating high-density water that cascades into 400 m basins in Barents Sea and into Nansen Basin, eroding sediments that form patches of turbid layers along slopes and in shallow basins. The weakness of bottom turbid layers in the deep basins is consistent with the lack of strong bottom currents.

Key Words:

Arctic Ocean

Transmissometer beam attenuation

Particle distribution

Particle sources

Nepheloid layers

1. Introduction

Because of seasonal to year-round ice cover, the Arctic waters have been less well studied than other oceans (Seidov et al., 2015). Global warming is decreasing the ice cover, making the Arctic waters more accessible. Technological advances in icebreakers and instrumentation, plus international collaboration have enabled significant expansion of exploration and discovery in the Arctic Ocean in recent decades. Further motivation for understanding conditions in the Arctic Oceans comes from existing plans and developments to extract hydrocarbons beneath the Arctic Ocean seafloor, and to access shorter shipping routes between the North Atlantic and Pacific oceans due to climate warming diminishing sea ice cover. Understanding the impact of increased human activity in the region requires that we record and understand present conditions and natural processes in order to predict and assess future impacts.

Optical instruments (e.g. transmissometers) can be used to determine the distribution of particulate matter (PM) and particular organic carbon (POC) in the ocean (Gardner et al. 1985; Mishonov et al., 2003; Boss et al., 2015). PM can act as a non-conservative, short-term tracer that can shed light on multiple processes occurring within the ocean; e.g. introduction of particles via rivers, biological productivity, and resuspension of bottom sediments. In situ sample collection by Xiang and Lam (2020) during the 2015 USCGC Healy GN01 cruise provides valuable information about the composition of PM and aides in calibrating our optical measurements. We examine the full water column data from the shelves and across the Arctic basins, focusing on surface and bottom regions. Optical measurements of chlorophyll-a fluorescence (Chl-a) helps identify biomass in surface waters or subsurface Chl-a maxima (SCM). Combining measurements of PM and Chl-a helps to roughly identify their first-order source (biogenic vs. terrigenous) in surface waters, subsurface maxima or intermediate and bottom nepheloid layers. In the open ocean (well beyond the shelf) in the Arctic as well as other oceans, below the euphotic zone and through the rest of the water column, PM is very low (Gardner et al., 2018a, b; Xiang and Lam, 2020) and Chl-a is near zero. Approaching the seafloor along margins or ocean basins, there can be an increase in PM which is identified as a nepheloid (cloudy) layer (Gardner et al., 2018a, b) that can result from local erosion and resuspension, or from lateral transport from a distal resuspension source. Active hydrothermal vents, where present, may also contribute particles.

In this paper we examine the distribution of PM together with distributions of Chl-a, sea water temperature, salinity, and nitrate along basin-wide transects by combining data from two simultaneous expeditions to the North Pole, coming

from opposite sides of the Arctic Ocean in 2015. This creates the first trans-Arctic section of optics-based particle distribution. Our goal is to offer a baseline of several PM parameters that are important in understanding the particle dynamics of the rapidly changing Arctic Ocean and discern the physical/biological processes that are most responsible for the PM and Chl-*a* distributions observed in different areas across the Arctic Ocean.

2. Methods

2.1 Ships, instrumentation and data processing

Data presented in this paper come from two expeditions on large icebreakers: the U.S. GEOTRACES (GN01) [ARC01] Expedition on the USCGC Healy (Kadko & Landing, 2015) and the PS94 Expedition on the German R/V Polarstern (Ober et al., 2016a, b; Rabe et al., 2016a, b; Schauer, 2016). Both ships started their voyages in mid-August, 2015, rendezvoused at the North Pole and at another station to sample simultaneously for inter-laboratory calibration of multiple sensors and parameters. Sampling continued for each ship along different routes back to their starting points, finishing in mid-October. We combined hydrographic and optical data from the two expeditions to make a basin-wide transect that crosses the entire Arctic Ocean from the Bering Strait, across the Chukchi shelf and Canada and Makarov Basins to the North Pole, and across Amundsen and Nansen Basins and the Barents Sea (Figure 1). The second transect is roughly parallel to the first transect from the Bering Strait across Makarov and Amundsen Basins to the Gakkel seafloor spreading ridge. For logistical reasons, the R/V Polarstern stations P147-P173 between 70°N and 75°N in the Barents Sea were occupied while steaming south at the end of the cruise, six weeks after the beginning of the poleward transect.

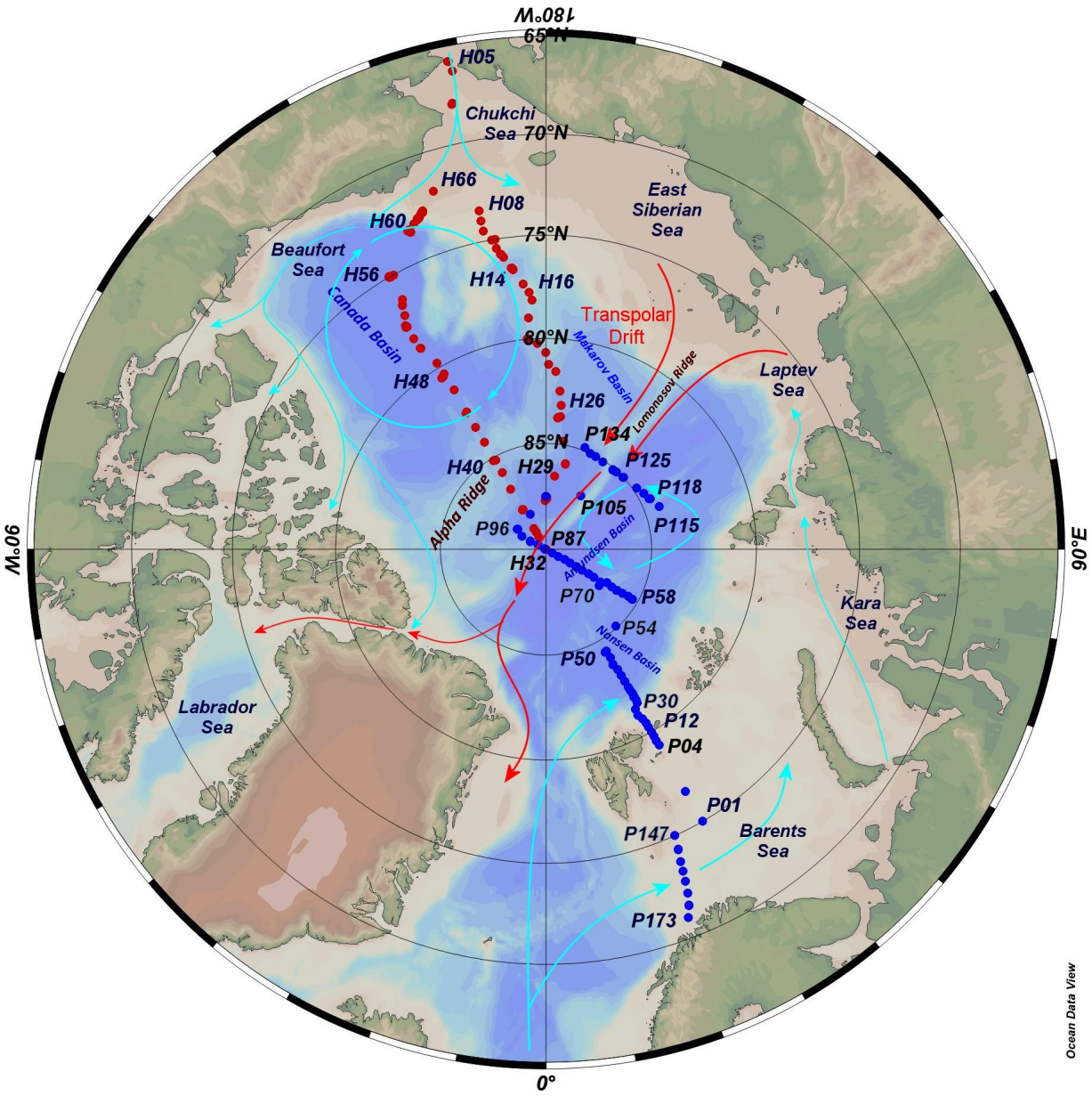

Figure 1. Map of Arctic Ocean and major circulation patterns with station positions of the USCGC Healy (from H05 to H66, red dots) and R/V Polarstern (from P01 to P173, blue dots). The large gyre in Beaufort Sea is the Beaufort Gyre. Light blue arrowed lines indicate general surface flow or circulation. Red arrowed lines indicate general flow of the Transpolar Drift (Flow lines after Charette et al., 2020).

Both ships were equipped with multiple CTD rosettes that included water collection bottles, WetLabs transmissometers, and either WetLabs or SeaPoint Chl-*a* fluorometers capable of reaching all depths in the Arctic Ocean. Xiang and Lam (2020) also had a CTD/WetLabs transmissometer package attached to a Seabird 19plus CTD deployed at the bottom of a string of large-volume in situ filtration pumps (100's of liters filtered per depth) during the USCGC Healy cruise. Their CTD/transmissometer functioned only on the northbound leg (i.e. stations H1 to H36), but other CTD/transmissometer casts were made at each of the pump stations for comparison with the filtration data.

The transmissometer beam attenuation coefficient due to particles (Cp) and fluorescence-based Chl-*a* measurements from both ships were recorded in volts and analyzed by the TAMU/UMD-NCEI group using the factory calibrations in the same manner as published in Gardner et al. (2018a). De-icing and cleaning transmissometer optical windows to obtain reliable air calibrations prior to each cast was not always possible in the field because of freezing weather conditions. Without reliable air calibrations from all transmissometers (a total of 6 instruments used on the two ships), the profile minimum signal found below 200 m from each deep-water cast for the open-ocean profiles, was set to zero. For stations with profiles less than 200 m depth we subtracted a cruise-average minimum value calculated based on all deep-water profiles. The Cp data are reported in units of m^{-1}. Sections of Cp are gridded and contoured with search radii of about 40 km along the transect and 20 m vertically. Original data from USCGC Healy expedition can be found at CCHDO data depository (expocode 33HQ20150809). Original data from R/V Polarstern can be found in PANGAEA datasets (http://doi.org/10.2312/BzPM_0703_2016 and http://hdl.handle.net/10013/epic.48723)

During the USCGC Healy expedition, Xiang and Lam (2020) collected size-fractionated particles at 2 to 24 depth levels (depending on water depth and available ship time) at 20 stations using large-volume in situ pumps. Hundreds of liters of water are pulled through a 51 µm polyester mesh and then though either paired 0.8 µm Supor polyethersulfone or paired 1 µm quartz fiber filters to collect size-fractionated (1-51 µm and >51 µm) particles. Major biogenic phases, including particulate organic carbon (POC), biogenic silica (bSi), and $CaCO_3$ were measured, as well as particulate trace metals, from which lithogenic and authigenic (Fe and Mn oxides) particle mass were estimated using methods described in Xiang and Lam (2020). PM was estimated as the chemical dry weight of the sum of all major particle phases in each size fraction. Please refer to Xiang and Lam (2020) for a complete description and discussion of the size-fractionated particle composition and concentration during the GN01 cruise.

2.2 Estimating Particulate Matter and Particulate Organic Carbon concentrations from Cp

The total concentrations of particles (>1 µm) from the full water column were derived from the sum of the two size fractions and were regressed against beam Cp (m^{-1}) from the USCG Healy expedition to estimate approximate conversion

factors between Cp and PM or POC. We use the term PM rather than suspended particulate matter (SPM) or total suspended matter (TSM) because, unless the particles are in a surface or bottom turbulent mixing layer, there is no suspending force impeding the gravitational descent of particles.

Concentrations of PM differed by one to two orders of magnitude between shelf and open ocean, so we separated the data into two groups of stations for the USCGC Healy expedition where in-situ filtration was conducted: those from the Bering Sea, Bering Strait, and Chukchi Shelf/Slope (stations H1-10 and H60-66), and those in the Canada, Makarov and Amundsen Basins (stations H14-H57, Figure 1). Regression slopes for PM/Cp were 1768 µg-m l^{-1} (shelf/slope) and 632 µg-m l^{-1} (open ocean Canada, Makarov and Amundsen Basins), and for POC/Cp, 87 µg-m l^{-1} (shelf/slope) and 238 µg-m l^{-1} (open ocean Canada, Makarov and Amundsen Basins) (Figure 2). For comparison, the PM/Cp slope values listed above bracket the value of 1208 µg-m l^{-1} calculated and used in our previous work to convert Cp to PM concentrations for global mapping of PM distribution throughout the water column (Gardner et al., 2018a).

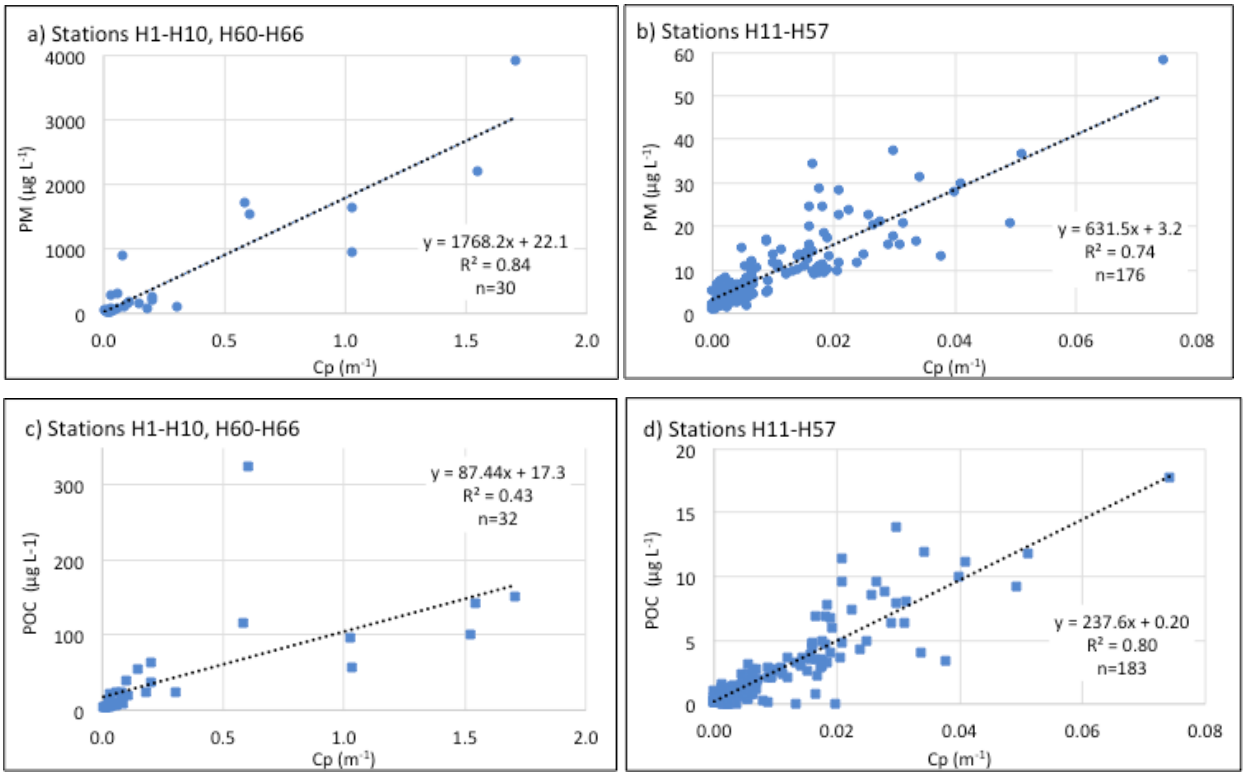

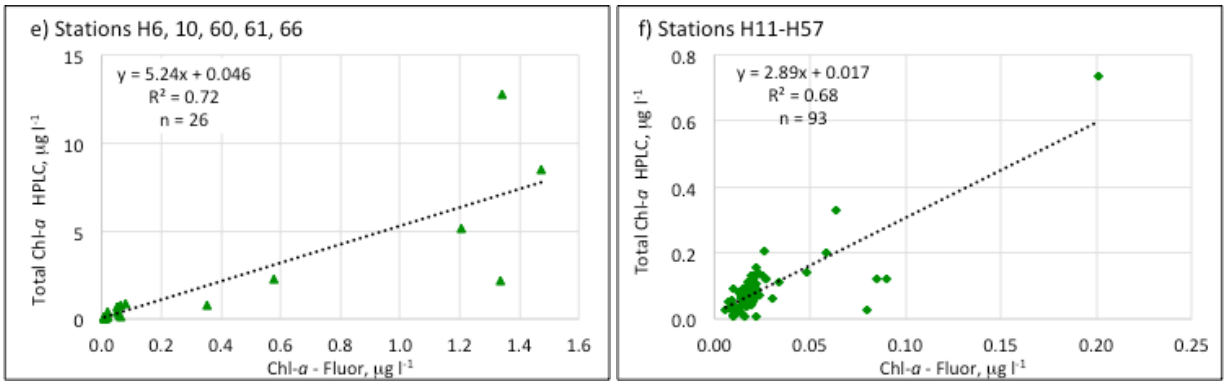

Figure 2. Linear regressions of Cp versus a) >1 µm PM sampled on the shelf and slope of the Chukchi Sea, b) >1 µm PM sampled in the open Arctic Ocean, c) >1 µm POC sampled on the shelf and slope of the Chukchi Sea, d) >1 µm POC sampled in the open Arctic Ocean. Note difference in scales. All PM and POC samples were analyzed by Xiang and Lam (2020). e) Linear regression of HPLC Chl- *a* versus fluorometer Chl-*a* on the shelf and slope, f) linear regression of HPLC Chl-*a* versus fluorometer Chl-*a* sampled in the open Arctic Ocean.

The smaller regression slope of POC/Cp compared with PM/Cp in both shelf/slope and open ocean environments in the Arctic Ocean indicates that a change in Cp reflects a smaller change in POC than in PM. Ohnemus et al., (2018) reported Cp/PM and Cp/POM (particulate organic matter) slopes of 1.73×10^{-3} $m^{-1}/(\mu g\ l^{-1})$ and 2.63×10^{-3} $m^{-1}/(\mu g\ l^{-1})$, respectively, for particles from the US GEOTRACES GP16 zonal transect in the Eastern Tropical South Pacific Ocean (ETSP). Taking the inverse of the Ohnemus et al. (2018) slopes and converting POM to POC based on the POM/POC weight ratio of 1.88 determined by Nuclear Magnetic Resonance (NMR) (Hedges et al., 2002) leads to an equivalent PM/Cp slope of 578 µg-PM m l^{-1} and POC/Cp slope of 202 µg-POC m l^{-1} in the ETSP. Thus, the open ocean ETSP regression slopes are more similar to our open ocean Arctic water (632 µg PM-m l^{-1} and 238 µg POC-m l^{-1}) (Figures 2b, d) than the shelf/slope regions of the Chukchi Sea (1768 µg PM-m l^{-1} and 87 µg POC-m l^{-1}) (Figures 2a, c). The highest PM concentrations in the ETSP were predominantly caused by surface and eastern boundary upwelling waters and did not exceed 140 µg l^{-1} (Lam et al., 2018), more similar to the PM ranges in the open Arctic Ocean (Figure 2b) rather than the shelf/slope regions (Figure 2a). However, it is not just total PM concentration that determines the variation in PM/Cp slopes, but also particle composition. A high abundance of lithogenic particles increases the observed PM/Cp regression slope. The high PM in the Chukchi shelf/slope regions of the Arctic Ocean was predominantly caused by resuspended lithogenic particles, accounting for >50% of PM (Xiang and Lam, 2020). Similarly, a higher PM/Cp slope was also observed in lithogenic-rich benthic nepheloid layers compared to biogenic-rich surface particle regimes of the ETSP (Figure 9 in Ohnemus et al. 2018).

In reality, there is no globally applicable slope for such regressions because of the variation in particle composition. In regions of the ocean where POC is the dominant component of PM, the relationship between Cp and POC is fairly constant (Bishop and Wood, 2008). The relationship between Cp and PM varies as a function of particle size, shape and composition (Baker and Lavelle 1984; Gardner, 1989; Boss et al., 2015), and can change with depth and source/composition of particles (biogenic versus lithogenic). For this reason, we plot beam Cp in units of m^{-1} rather than applying a single conversion factor to obtain PM. As a rough estimate drawn from these plots, a $0.1m^{-1}$ increase of Cp is approximately equal to 177 µg l^{--1} increase in PM on the shelf and 63 µg l^{-1} in the open Arctic Ocean. For POC, a 0.1 m^{-1} increase of Cp is equal to approximately 9 µg l^{-1} increase on the shelf and 24 µg l^{-1} in the open Arctic Ocean. Given that POC concentrations decrease rapidly with depth through remineralization, the Cp equivalents in POC units are expected to be smaller in deep water where POC concentrations are very low.

2.3 Estimating Chl-*a* from fluorometers

All CTD packages were equipped with either a WetLabs (excitation/emission at 470/695 nm wavelengths) or SeaPoint (excitation/emission at 470/685 nm wavelengths) Chl-*a* fluorometer. The factory Scale and Dark values were used in standard SeaBird SeaSave software for data reduction and the data were recorded as fluorescence-based Chl-*a* *(*µg l^{-1}). Both manufacturers point out that their Chl-*a* fluorometers are calibrated with a specific phytoplankton type at the factory. The optical fluorometer measurements on the CTD provide much higher vertical and horizontal resolution than bottle data. Water samples were drawn from the upper 100 m for High Performance Liquid Chromatography (HPLC) measurements at 27 GEOTRACES stations on the USCGC Healy. There are no HPLC measurements from the R/V Polarstern. Fluorometer Chl-*a* data from the two expeditions had a constant offset relative to each other with R/V Polarstern data having elevated values (about 0.015 µg l^{-1}) compared to USCGC Healy data. This may have resulted from a difference in fluorometer brands, the phytoplankton species used for factory calibration, or the 10nm difference in emission wavelength. To make Chl-*a* data from two expeditions comparable we performed data adjustment similar to Cp data processing, using deep-water Chl-*a* minima as a reference point for each profile.

Chl-a has become a universal parameter for estimating phytoplankton biomass and productivity (Bidigare et. al. 2005; Roesler et al., 2017). Just as transmissometer beam attenuation depends on particle composition, so Chl-*a* fluorescence also changes with natural variations in phytoplankton carbon to Chl ratios of different species and plankton photo acclimation conditions (Roesler et al., 2017). They also noted that point by point comparisons for paired HPLC and in-situ factory-calibrated Chl-a fluorescence measurements yield large scatter unless the data sets are restricted spatially and/or temporally due to the variability in plankton species, light intensity, and plankton in vivo activity. They define the ratio between the factory-calibrated in-vivo fluorescence-derived

Chl and the HPLC-derived Chl as a dimensionless "slope factor." This slope factor varies regionally between 1 and 6 for the major oceans they tested. For the Iceland Basin they reported a slope factor of 2.5 from a profiling float and 1.3 based on data from Coupel et al., (2015), although only HPLC chlorophyll measurements are given in Coupel et al., (2015). Our slope factors are about 5 on the Chukchi shelf/slope where conditions are highly variable and about 3 for the stations sampled in the open western Arctic ocean (Figure 2e, f). We did not identify or remove observations impacted by non-photochemical quenching (Roesler et al., 2017).

3. Hydrographic setting

Detailed descriptions of the seasonal and regional hydrography and currents of the Arctic Ocean can be found in Jones (2001), Rudels et al., (2004), Steele et al., (2004), Seidov et al., (2015), and Timmermans and Marshall (2020). Our discussion will focus on conditions and processes along the two transects from mid-August to early October, 2015.

The above authors documented how the Arctic Ocean is fed from both the Pacific and Atlantic oceans, with water exiting along several routes to the North Atlantic. They also emphasize that in the cold water of the Arctic Ocean, salinity is the major control of density, not temperature as is the case at lower latitudes. Thus, the Arctic Ocean has haloclines that control stratification much more than thermoclines. Pacific water enters through the Bering Strait, also bringing sediment, nutrients and water from the Yukon River (Roach et al., 1995; Jones et al., 2003). Pacific water density is greater than the low-salinity surface polar mixed layer (PML) that contains fresher water from annual melting of sea ice plus fresh water outflow from Arctic rivers, for example Canada's Mackenzie River east of Barrow, Alaska, and several rivers from the East Siberian Sea along northern Russia.

Most of the Pacific water sinks beneath the PML as it moves off the Chukchi Shelf, forming what is known as Pacific halocline water (Rudels et al., 2004). To define the Pacific halocline water, Timmermans and Marshall (2020) use a potential density range of 25 – 27.4 kg m^{-3}, which corresponds to salinities of approximately 31-34. Pacific halocline water rests on top of the denser Atlantic halocline water entering from the Atlantic Ocean through the eastern side of Fram Strait and through the Barents Sea in the eastern Arctic Ocean. While much of the Pacific Ocean water is entrained in the predominantly anticyclonic flow of the Beaufort Gyre in the Canada Basin, some of it exits the Arctic Ocean through the west side of Fram Strait into the Greenland Sea (Rudels et al. 2004). Water in the Beaufort Gyre contributes to the Trans-Polar Drift (TPD) from East Siberian and Laptev Seas across the pole area and either continues circulating in the Beaufort Gyre or exits the Arctic Ocean through the Canadian Archipelago or through the west side of Fram Strait (red and light blue arrowed lines respectively on Figure 1).

Water entering through Barents Sea encounters irregular topography including

small basins ranging in depth between ~100 m to 450 m. Strong winds during winter storms cool the relatively warm, salty water, some of which cascades down into these small, medium-depth basins or into the Arctic basin to form the Atlantic halocline water starting in the Nansen Basin and spreading across the Arctic Ocean (Ivanov et al., 2004). Several large rivers also feed into the Arctic Ocean along the northern Siberia margin carrying sediment and nutrients as well as fresh water.

Sea ice covers most of the Arctic Ocean in winter, though much of the Barents Sea is ice-free year round. The area of permanent sea ice has diminished significantly in recent years, causing changes in hydrologic and biological cycles (Perovich et al., 2019). By August there is no ice cover in the Barents Sea out to the edge of the Nansen Basin (Fetterer et al., 2017). Over on the Pacific side of the Arctic Ocean, winds and currents move Pacific Ocean water through the Bering Straits, melting annual ice and pushing ice out of the Chukchi Sea and into the Beaufort Gyre in the summer and fall. Ice thickness along the USCGC Healy track was generally ~1-2 m (Healy ship logs) and along R/V Polarstern tracks ice thickness was a mean of 1.6 m. (Schauer, 2016, Figure 4.5). The presence of ice is schematically given at the top of Figures 3, 4 and 6.

4. Distribution of Cp, Chl-*a*, salinity, and temperature for the trans-Arctic sections.

4.1 Arctic Ocean sections

Cp distributions along the trans-Arctic sections are shown by the color scales in Figures 3 and 4. Contours of salinity, temperature and Chl-*a* are overlain on the Cp sections. Cp can be converted to PM or POC using the equations in Figure 2.

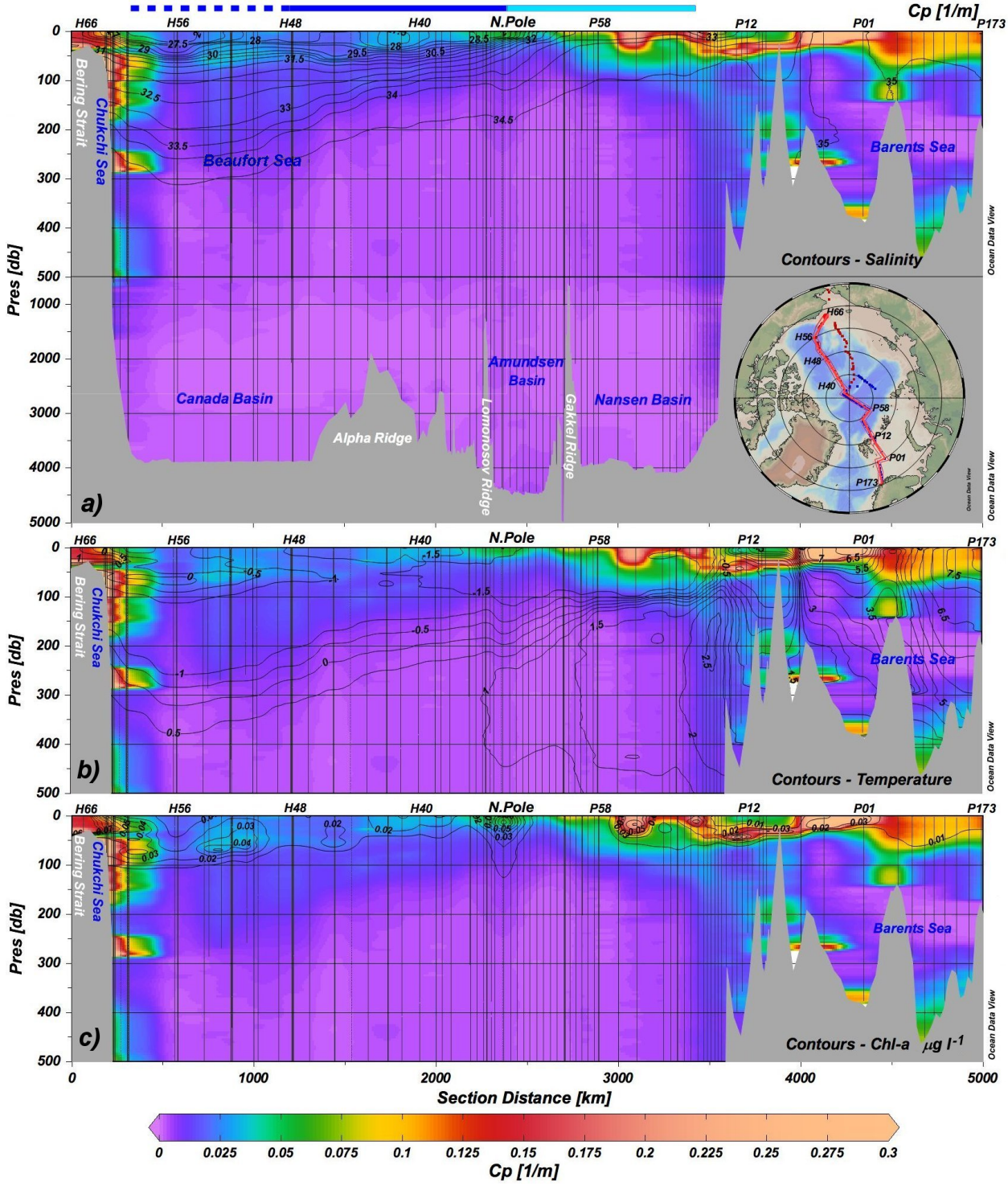
Cp [1/m]
H66
H56
H48
H40
N.Pole
P58
P12
P01
P173
Pres [db]
Bering Strait
Chukchi Sea
Beaufort Sea
Barents Sea
Canada Basin
Alpha Ridge
Amundsen Basin
Lomonosov Ridge
Gakkel Ridge
Nansen Basin
Contours - Salinity
a)
b)
Contours - Temperature
c)
Contours - Chl-a µg l-1
Ocean Data View
Section Distance [km]
0
0.025
0.05
0.075
0.1
0.125
0.15
0.175
0.2
0.225
0.25
0.275
0.3
Cp [1/m]

Figure 3. The transect of Cp (color scale; proxy for PM or POC from Figure 2) from Bering Strait via North Pole to Norway with contours of a) Salinity, b) Seawater temperature, °C), and c) Fluorescence-based Chl-*a*, µg l^{-1}. Blue lines at the top schematically represent the sea surface ice condition: dashed line indicates the area along which ice cover increased from 20% to 80%, bold blue line represents area covered by >80% ice, light-blue line indicates ice-covered area reported by Schauer (2016; Figure 4.1) for R/V Polarstern expedition, no line represents relatively ice-free area. The color scale is in units of beam attenuation coefficient due to particles, Cp (m^{-1}), Vertical lines are station locations (or 1000 km markers) and the labels above each frame are station numbers (*H* for Healy, *P* for Polarstern). Some station lines appear thicker because multiple casts were made there. The cruise map in the top panel indicates the stations along orange lines used in the section. We use the section distance for the X-axis. Note the Y-axis (pressure) scale change at 500 db (panel a).

Cp is highest in Chukchi and Barents Seas, especially where there is no ice cover. Surface Cp in Nansen Basin is higher than in Amundsen, Canada or Makarov Basins. There is deeper penetration of particles (Cp) in the Canada and Makarov Basins than in Amundsen and Nansen Basins and Barents Sea basins and Cp values tend to follow the deeper salinity (Figures 3a, 4a) and temperature contours (Figures 3b, 4b) in Canada and Makarov Basins compared to Amundsen and Nansen Basins. In surface waters Chl-*a* follows the Cp contours (Figure 3c), suggesting that primary production makes up a dominant portion of the particle concentration, except between stations P115-P134 (Figure 4c). The lack of overlap in that area of Figure 4c could be an impact of the TPD bringing either lithogenic particles from the Siberian region or old detrital POC that no longer fluoresces.

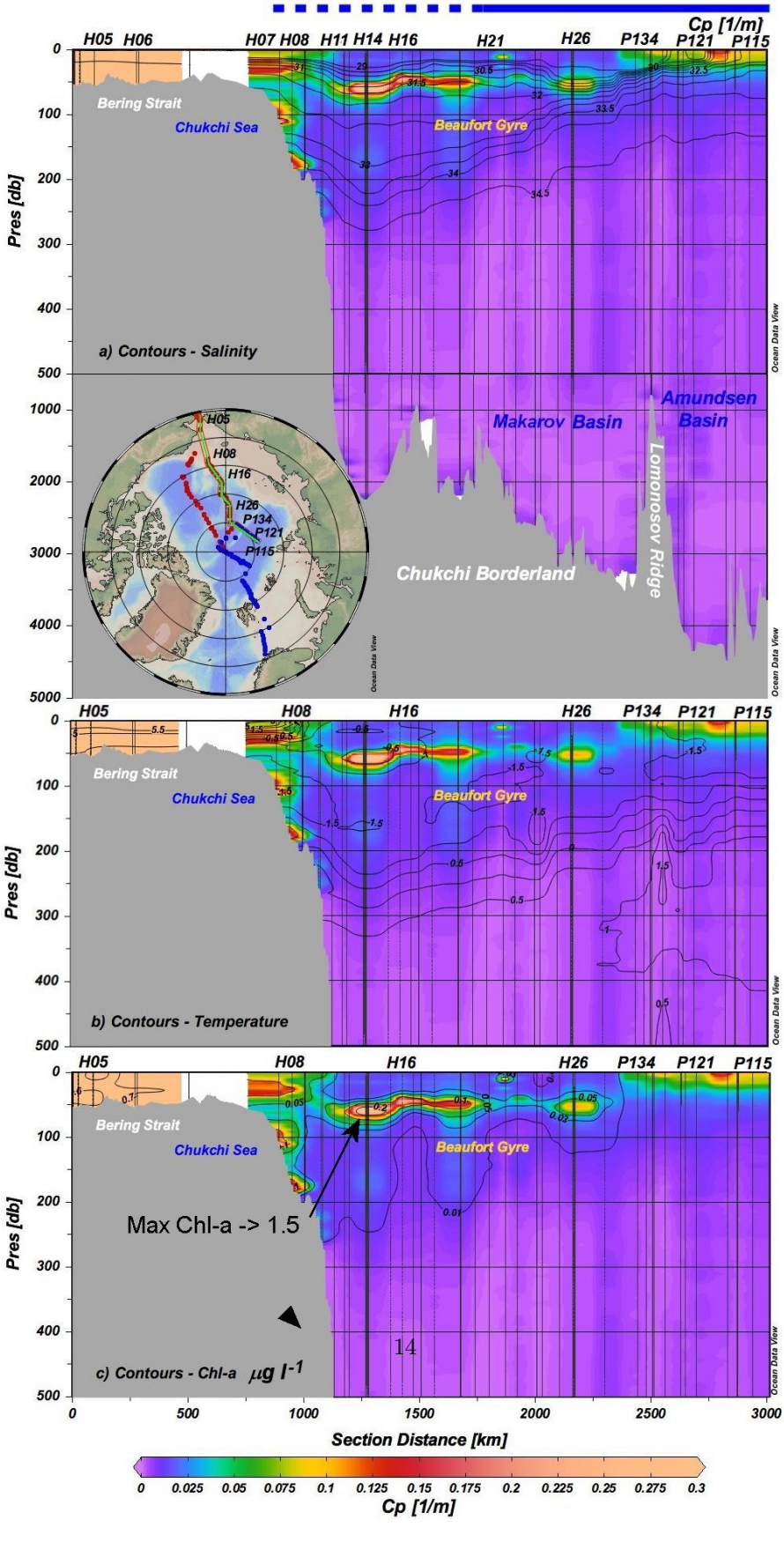
Cp [1/m]
H05 H06 H07 H08 H11 H14 H16 H21 H26 P134 P121 P115
Bering Strait
Chukchi Sea
Beaufort Gyre
Pres [db]
a) Contours - Salinity
Makarov Basin
Amundsen Basin
Lomonosov Ridge
Chukchi Borderland
Ocean Data View
b) Contours - Temperature
Max Chl-a -> 1.5
c) Contours - Chl-a µg l-1
Section Distance [km]
0 0.025 0.05 0.075 0.1 0.125 0.15 0.175 0.2 0.225 0.25 0.275 0.3
Cp [1/m]

Figure 4. The semi trans-Arctic transect (see green line on map inset) of Cp (color scale) from Bering Strait to Amundsen Basin (Northbound) with contours of a) Salinity, b) Seawater temperature, °C), and c) Fluorescence-based Chl-*a* in µg l^{-1}. See Figure 3 caption for details.

4.2 Distribution and controlling processes of PM (Cp) and Chl-*a* on the shelf of Chukchi Sea, and upper 500 m of the open ocean Beaufort Sea

Filtration sampling by Brewer et al. (1976) in the Atlantic Ocean, and our own measurements made around the globe (Gardner et al., 2018 a, b) show minimum PM concentrations in the water column within the range of about 5–12 g l^{-1}. Minimum concentrations of total PM recorded during this Arctic expedition from in-situ pump filtration were in the range of about 1-7 µg l^{-1} (Xiang and Lam, 2020), which is lower than typical clear water minimum concentrations in the GA03 North Atlantic cruise (~5 µg l^{-1}) or in the GP16 Eastern Tropical South Pacific cruise (~4 µg l^{-1}) estimated by the same methods (Lam et al., 2015a, b; Lam et al., 2018). The smaller minimum concentrations may result from lower surface primary production in ice-covered waters, as suggested by Honjo et al. (2010). In Arctic surface waters, PM concentrations measured from the pump samples ranged between 10's-100 µg l^{-1}, whereas in benthic nepheloid layers in Bering Strait, on the Chukchi shelf, and upper slope PM concentrations ranged between 100's to >1000 µg l^{-1} (Xiang and Lam, 2020).

Sediment and abundant nutrients from the Yukon river south of the Bering Strait join with Pacific water and are brought into the Arctic Ocean through the 40-50 m deep strait (Nelson and Creager, 1977; Roach et al., 1995; and Jones et al., 2003). Several studies have sought to unravel how the Pacific water crosses the Chukchi Shelf. Spall et al., (2018) identify three key locations where the transport occurs: Barrow Canyon, the Beaufort shelf break, and the Chukchi shelf break and slope, with most of the water eventually passing through Barrow Canyon and then turning to the west to form the Slope Current (Corlett and Pickart, 2017; see Section 6 for fuller discussion of currents and sediment transport in the Chukchi Sea and benthic nepheloid layers throughout the Arctic). Spall et al., (2018) state that it is a complicated, non-linear system involving a wind-driven anticyclonic gyre and flow exiting Barrow Canyon that is driven by variable flow through Bering Strait. It is possible that some of the variable flow in Barrow Canyon is the effect of internal tides causing the water to move up and down the canyon as observed in other canyons (Hunkins, 1988, Gardner, 1989; Puig et al., 2013).

Other studies have shown that eddy transport can contribute to the transfer of water, sediment and nutrients from the Chukchi shelf to the Beaufort Sea (Mathis et al., 2007; Kadko et al., 2008; Watanabe et al., 2014). During this expedition the Healy's Acoustic Doppler Current Profiler was used to measure currents and eddies in the upper 400 m of the water column. Eddies were detected in the upper 200 m between stations H14-H18, however, high Cp (Cp is 0.05-.17, so POC ~12-40 µg l^{-1}) and elevated Chl-*a* (Chl-*a* max is 1.5 µg l^{-1} at 60 m at station H14) in that area suggest that marine biogenic matter is produced

in-situ in this region (Figure 4c). The Northbound section (Figure 4a) over the Chukchi borderlands shows elevated bottom/intermediate nepheloid layers centered on the slope at both 100 and 180 m depth (stations H07-H08), with lower intensity layers between 200-300 m depth (stations H09-H11). Abundant Chl-*a* was present on the shelf in the regions of high Cp, and Chl-*a* was associated with small intrusions of high Cp on the upper slope between about 100-200m.

Conditions in crossing the Chukchi slope along the Southbound section (Figure 3c) are a little different. There are several layers along the slope with varying intensities of Cp down to 600 m (see Figure 3a), but Chl-*a* >0.01 µg l^{-1} appears only in the shelf plume (<100 m, Figure 3c). Some water coming through the Bering Strait leaves the shelf near this transect as the Alaska Coastal Current and flows over Barrow Canyon (Corlett and Pickart, 2017). They found that the Coastal Current not only bends to the right (i.e. southeastward) to form the Shelfbreak Jet, but also splits to the left (i.e. northwestward), forming the Slope Current (Figure 5). The low Chl-*a* values in the deeper layers (100-500 m), suggest that most of the PM in the slope nepheloid layers is non-living, likely resuspended sediment advected either along slope or seaward. Strong evidence of the dominance of non-living, resuspended sediment in the slope nepheloid layers comes from data and analysis of Xiang and Lam (2020). Particles at the intermediate nepheloid layer at station H61 are characterized by 70% lithogenic material, with the remainder divided between opal (~20%), POM (~7%) and Fe oxides (~3%), indicating resuspension of surface sediments composed primarily of lithogenic material with some aged biogenic and authigenic material. Previous Arctic studies have proposed lateral transport of sediment from the shelf and slope based on sediment trap studies (Honjo et al., 2010; O'Brien et al., 2013; Hwang et al., 2015) or direct sampling of water in those regions (Xiang and Lam, 2020).

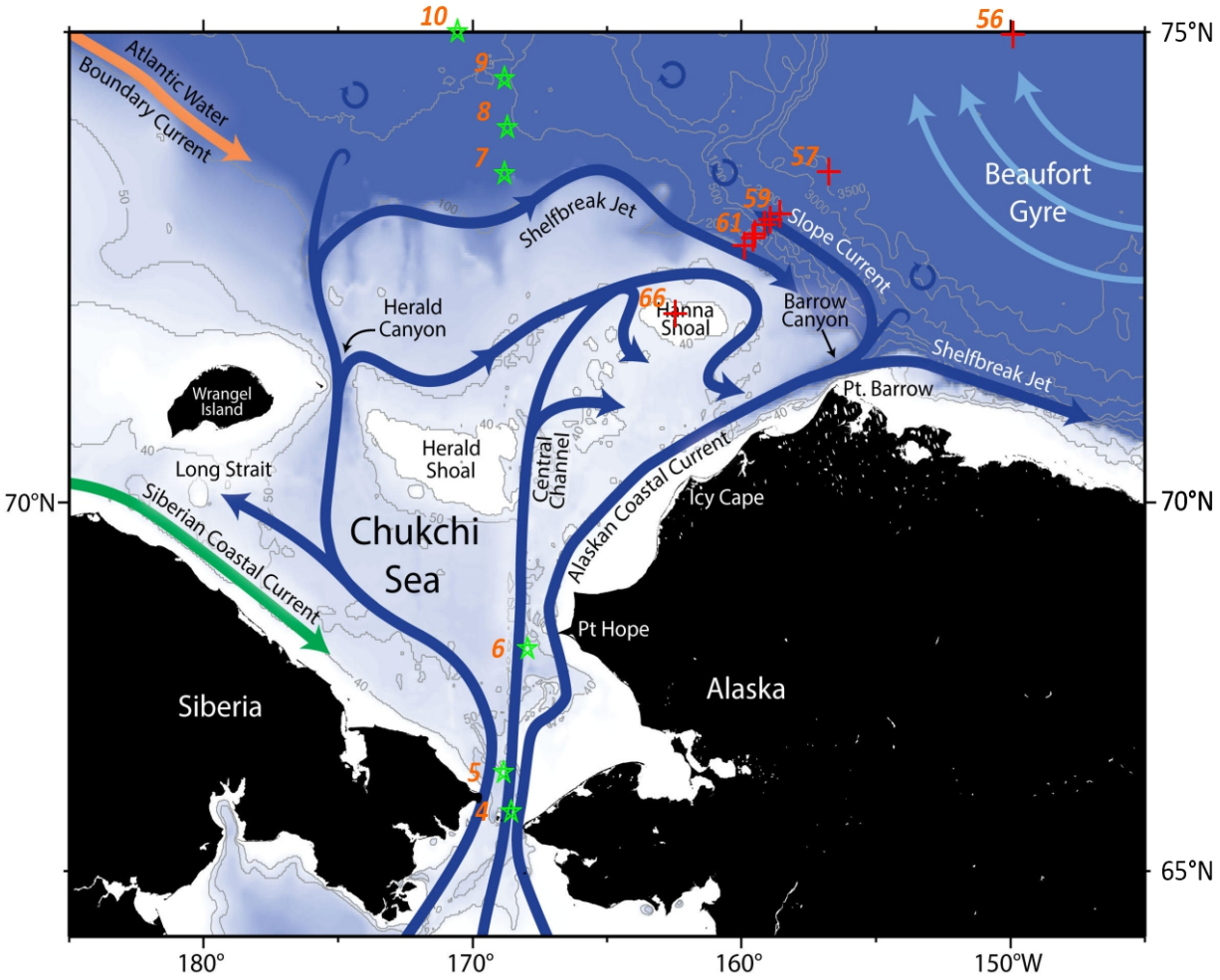

Figure 5. Stations along the semi Trans-Arctic transect (green stars; corresponds to Figure 4) and Trans-Arctic transect (red pluses; corresponds to Figure 3) overlain on a bathymetric map showing the schematic circulation in the Chukchi Sea and western Arctic Ocean (modified from Corlett and Pickart (2017)).

Rudels et al. (2004) and many other authors have described the Pacific halocline layer that flows off the Chukchi Shelf (Figure 3a) and borderland (Figure 4a) into the Beaufort Sea. Timmermans and Marshall (2020, Figure 3) suggested that Pacific halocline waters fall between a potential density of 25 – 27.4 kg m^{-3}, corresponding with a salinity of 31-34. This fits well with our 2015 data where maximum halocline water depth was at about 250 m at stations H14 (Figure 4a) and H56 (Figure 3a), and shoaling up to the base of the PML in the vicinity

of the North Pole (Figures 3a, 4a). The deep penetration of particles in both the Canada (Figure 3) and Makarov (Figure 4) Basins coincides with the depth of the Pacific halocline. Several particulate chemical tracers, including ^{13}C-POC, MnO_2, and elevated biogenic Si point to a shelf origin of particles found in the Pacific halocline layer in the Canada and Makarov Basins (Xiang and Lam, 2020; Jensen et al., 2020), suggesting that the elevated Cp signal down to the Pacific halocline might be at least partly derived from lateral transport from the shelf, with exact mechanisms of transport requiring further research. Possible mechanisms and evidence of cross-shelf transport are discussed further in section 6.4.

4.3. Subsurface Chl-*a* Maxima.

Subsurface Chl-*a* Maxima (SCM) have been observed regularly in the Arctic Ocean (Ardyna et al., 2013; Steiner et al., 2016). In both transects (Figures 3c, 4c) we observe SCMs of varying intensity between about 30 m -70 m depth. Cp values are also elevated in those regions. The PML thickness is typically 25-50 m in winter and 5-30 m in summer (Peralta-Ferriz & Woodgate, 2015; Toole et al., 2010). The low-density PML strongly inhibits upward mixing of nutrient-rich halocline waters with surface waters. Nitrate concentrations in the mixed layer in Canada, Makarov and Amundsen Basins were usually less than 0.5 µM, but were between 0.5 - 4 µM in the Nansen Basin and Barents Sea (Figures 1 and 6). Landry et al., (1998) found that primary production in the open ocean becomes limited when nitrate is below 0.5 µM. The lack of nutrients in the mixed layer and light reduction due to sea ice explain the low surface Chl-*a* and Cp in the strongly stratified western basins. The higher values of nitrate in the eastern Arctic Ocean (including Barents Sea) results in higher Chl-*a* and Cp where water is less stratified and has less sea ice cover (Figure 3c). Light sufficient for primary production can penetrate deeper than the average mixed layer thickness, so when nutrient concentrations exceed 0.5 µM, SCMs can develop at varying depths and intensities depending on the availability of nutrients and light, both of which vary spatially and temporally with ice and mixed layer thickness. Ideally the photosynthetically active radiation (PAR) sensors on CTD hydrocasts could be used to estimate the depth of the euphotic zone (Lee et al., 2007), but no PAR data were reported for stations H11- H25. Limited PAR data for stations H26-56 yielded 1% light levels around 80-100 m, which is much deeper than the mixed layer and enables formation of SCMs where nutrients are available. Figure 6 shows insufficient nitrate for significant photosynthesis in surface waters between stations H07 and H26 and stations H40-H57 in the western Arctic, but sufficient nitrate and light for photosynthesis in some surface waters east of the North Pole.

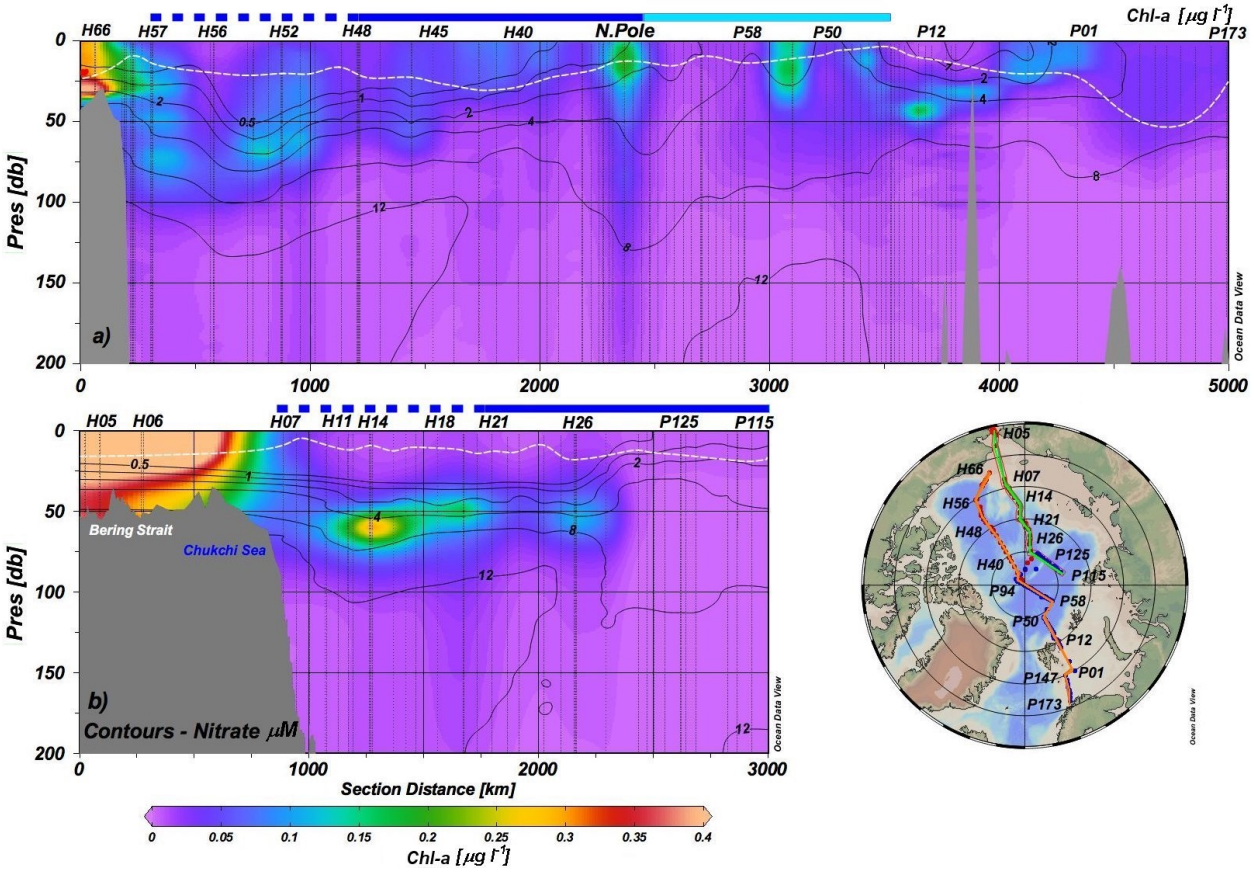

Figure 6. Sections showing fluorescence-based Chl-*a* (µg l^{-1}) in color scale with black contours showing nitrate concentrations (µM) for: a) Trans-Arctic section (orange line), and b) Semi trans-Arctic section (green line). Dashed white lines represent mixed layer depth estimated following Lorbacher et al., (2006), as closest to the surface depth of the second derivative maximum of the density profile. Blue lines at the top schematically represent the sea surface ice condition: dashed line indicates the area along which ice cover increased from 20% to 80%, bold blue line represents area covered by >80% ice, light blue line indicates ice-covered area reported by Schauer (2016; Figure 4.1) for R/V Polarstern expedition, no line indicates ice-free area. Ice thickness was generally 1-2 m.

SCMs are present in both sections (Figures 3c, 4c, 6). Between stations H11 and H26 (Figure 4c) the SCM is at about 50 m -70 m and might be interpreted as an extension of input from the shelf, but the high Chl-*a* values are evidence that in-situ primary production is more likely (Figure 4c). Measurements of Ra-228 by Kipp et al., (2019; their Figure 2) show a layer of Ra-228 which traces back to the Chukchi shelf. That Ra-228 layer is generally coincident with the high Chl-*a* area (Figures 4b, c). Kipp et al. (2019; 2020) explain that the only

plausible source of Ra-228 far from the shelf is the pore-waters of resuspended shelf sediments. They also state that the pore waters that supply Ra-rich water could also provide nutrients that would enhance primary production in-situ. The nutrient-rich water carried seaward by internal waves (Cacchione and Drake, 1986), currents, or eddies could also enhance primary production of Chl-*a* along that pathway. A similar overlap between the SCM and Ra-228 exists between stations H46 – H56, suggesting possible nutrient transport off this region of the Chukchi Shelf and enhanced in-situ production creating an SCM. In both cases the Ra-228 layer extends down to about 200 m, but elevated Chl-*a* extends to only ~70 m, which was likely near the maximum depth of the euphotic zone since nitrate was abundant below 70 m (Figure 6), i.e., primary production at that depth was light limited, not nutrient limited.

Both SCMs and surface Chl-*a* highs, occur at varying depths in the upper 50 m in the Barents Sea between 3000 and 4500 km along the Trans-Arctic section (Figures 3c, 6a). Much of the Barents Sea has limited ice cover with less stratified water and in some areas a thicker mixed layer (Figure 6), which allows deeper mixing, bringing subsurface nutrient-rich waters into the euphotic zone. Chl-*a* is a small component of the total carbon biomass of phytoplankton. Carbon-to-Chl -*a* ratios in a 24-year study in Danish coastal waters averaged about 15:1 in winter and increased to 20:1 to 96:1 in summer (Jakobsen & Markager, 2016). The ratio depends on phytoplankton species composition, nutrient concentration and light intensity of the environment. Behrenfeld and Boss (2006) showed that Cp is linearly related to Chl-*a* concentration in well-mixed, biologically homogeneous, open-ocean surface waters. In our data we see that Cp is related to the total particle mass, and in surface open-ocean waters is closely related to the POC concentration (Figure 2d). Furthermore, the highs and lows in Chl-*a* contours match highs and lows of Cp in Barents Sea (Figure 3c), suggesting that POC and PM concentrations in surface waters are driven by primary production with some constraint by salinity stratification. The Arctic is far more variable physically and biologically than the area sampled by Behrenfeld and Boss (2006). Although we find Cp/Chl-*a* linearity at individual stations away from margins in the open Arctic, there is no single comprehensive correlation applicable across the entire region. Near continental regions in the Arctic, a likely reason is the high variability of both POC and lithogenic particles. In any case, primary production in surface waters increases both Chl-*a* and total Cp.

Assuming that the eastern Arctic basins have a similar relationship between Cp and POC or PM as the western Arctic basins (Figure 2), optically-derived POC or PM concentrations in surface waters are up to eight times greater in the Nansen Basin and Barents Sea (maximum Cp of 0.25 m^{-1}) than in most of the Canada Basin (maximum Cp of 0.03 m^{-1} in most of Canada Basin, Figure 3a). Although this is a reasonable assumption, filtered water samples from Nansen basin would have verified or negated the assumption of similar relationships between Cp and POC and PM. The combination of filtered particle analysis with optical measurements demonstrates the advantage of having both types of measurements to determine particle sources in the ocean. Calibrating

optical particle measurements with particle composition based on filtered samples greatly increases the ability to map particle distributions spatially and to identify particle sources.

Xiang and Lam (2020; their Figure 7) used ^{13}C-POC and a two end-member mixing model to estimate that the small size fraction of POC below 100 m depth in the western Arctic basin is comprised of a mixture of vertically settling and laterally transported POC. Even in the middle of the basin, they estimated that up to 40% of POC is from lateral advection, which is consistent with observations made by Honjo et al. (2010).

An unusual SCM was observed near the North Pole (Figures 3c, 6a). Surface salinity was <30 and the nitrate value from a surface bucket sample was zero. Salinity increased to 31 by 20 m depth. Nitrate was 2 - 4 µM between 20 m and 60 m and continued increasing to 200 m (Figure 6a). Chl-*a* reached a maximum of 0.2 µg l^{-1} at 20 m, and decreased with depth down to 250 m in four separate profiles (not shown). Since 250 m is well below the euphotic zone, we assume that some fresh phytoplankton was sinking to that depth before being consumed by grazing zooplankton. While traversing the gut of zooplankton, Chl-*a* is converted to pheophorbide and pheophytin (Strom, 1993) and would not add to the Chl-*a* signal. Slagter et al., (2017, Figure 1), Charette et al. (2020) and Rutgers van der Loeff et al., (2018) measured several parameters including DOC, CDOM fluorescence, Ra-228, Nd, and dFe during the 2015 field work and concluded that the Trans Polar Drift path happens to cross over the North Pole area, so the water carried by the Trans Polar Drift is the likely cause of these anomalies.

5. PM distribution from Cp and processes in the Barents Sea and Atlantic halocline

The Barents Sea consists of numerous shallow basins whose topography is highly exaggerated in our figures. High salinity (>34.5), warm (up to 8°C) Atlantic water from the Norwegian Sea moves into the area (Figure 3). Much of the Barents Sea has no seasonal ice cover, especially south of Svalbard, so strong, cold winds cool the salty water quickly, causing cascading of cold, dense water into the shallow basins of Barents Sea and eventually moving into Nansen Basin where it joins with Norwegian Sea water coming through the eastern side of Fram Strait.

Surface waters in the Barents Sea and Nansen Basin had similar Chl-*a* values to those in surface waters of the Canada, Amundsen, and Makarov Basins at this time of year (Figure 6), but the Cp values (Figure 3) were much higher in the Barents Sea and above Nansen Basin. The strong match between Chl-*a* contours and Cp values suggests a possible correlation with biomass concentrations in these surface waters (Figure 3c). Conversely, the high values of Cp near the sides or bottom of small basins in the Barents Sea show no Chl-*a*, so those high Cp values are most likely due to lithogenic sediment being resuspended by cascading of cold, hypersaline water. The close station sampling on the Barents

Sea / Nansen Basin border reveals a gradual decrease of Cp with distance as well as depth from the Barents Sea slope. This is roughly the boundary of multi-year ice moving south into the Atlantic Ocean through Fram Strait (Timmermans and Marshall, 2020).

Although the water entering Nansen Basin from the Barents and Norwegian seas is warmer than water in the Pacific halocline, its salinity (>35), and therefore density (>27.5), are greater than the Pacific halocline water, so it sinks below the Pacific halocline water as it spreads into the Arctic Ocean where it interleaves and mixes with colder water as seen in the temperature contours in Figure 3b.

6. PM distribution in deep Arctic Basins and along continental margins

6.1 Benthic Nepheloid layers in Arctic Basins

Prior to the time when icebreakers were available for Arctic Ocean research, the ice pack served as the scientists' "ship" as the wind and currents moved their ice camps around the Arctic Ocean and they sampled where the ice took them. Between 1965 and 1969, Hunkins et al., (1969) collected 51 nephelometer profiles (turbidity sensor; Thorndike and Ewing, 1967) through the water column to the seafloor while drifting from Canada Basin, northwest to the Mendeleev Ridge and then north across Alpha Ridge. The early version of this film-recording nephelometer was not calibrated in absolute terms, but it gave relative measurements of turbidity that they tried to relate to PM concentration. The nephelometer film was saturated by solar light in the upper 250 m (therefore no data), below which light scattering intensity generally decreased with depth. The clearest waters occurred at about 2000 m. If there was an increase near the bottom, it was viewed as a benthic nepheloid layer that contained resuspended sediment. Profiles in Canada Basin rarely showed any bottom nepheloid layer. A spot measurement of bottom current at that time was ~1 cm s^{-1}. Moderate nepheloid layers were found in the Chukchi Borderland north of the Chukchi Sea and along the Mendeleev and Alpha ridges. Four spot current measurements along Mendeleev ridge were 4-6 cm s^{-1}, which is below the threshold for fine-sediment resuspension (Miller et al., 1977). For calibration of light scattering, a few 200-liter near-bottom samples were centrifuged and filtered at stations where nephelometer profiles were taken. After filters were weighed in the lab, calculated PM concentrations were about 6-10 µg l^{-1} in the clear water (n=2) and about 8-10 µg l^{-1} near bottom (n=3) (Hunkins et al., 1969), a difference that is indistinguishable.

Based on a global compilation of benthic nepheloid layers, particle concentrations range from low (10's µg l^{-1}) to high (100s-1000s µg l^{-1}) with nepheloid layers being meters to over a kilometer in thickness (Gardner et al., 2018a, b). The increase can result from local erosion and resuspension by currents or activity of benthic organisms, but for nepheloid layers thicker than the benthic boundary layer (10-100 m), the increase in PM must result from resuspension along shallower seafloor followed by lateral advection, or cascading from cold, dense water sinking and eroding/resuspending sediment as it descends along the

sloping seafloor.

Jackson et al. (2010) used optical instruments to study the distribution of PM and Chl-*a* in the Canada Basin from 2003 to 2008 and observed the highest light attenuation, POC, and PM values along the Beaufort shelf and the lowest values were located along the eastern shelf of the Canada Basin. While sampling methods have improved tremendously since the early nephelometer era, the general results of the distribution and magnitude of nepheloid layers in the deep Arctic Ocean are quite similar (Jackson et al., (2010) and this paper). The clearest water is still found around 2000 m depth, below which PM increased by only a few micrograms per liter at most stations.

The large-volume in-situ filtration from USCGC Healy in 2015 yielded total PM concentrations in a range of 1-7 µg l^{-1} in the clearest mid-water regions and 3-7 µg l^{-1} in deep basins. While the nepheloid layer increases are very small in Cp units (Figures 3 and 4), concentrations of particulate aluminum show a distinct, if modest, increase caused by resuspension of lithogenic sediment in bottom waters (Xiang and Lam, 2020). Indeed, the modest near-bottom enhancements in measured PM are comprised primarily of lithogenic particles. The relative insensitivity of Cp to the Arctic nepheloid layers is a reflection of the generally lower sensitivity of Cp to lithogenic particles compared to other particle types such as POC (Ohnemus et al., 2018) and the low absolute PM concentrations (<10 g l^{-1}) found in some Arctic nepheloid layers. Analysis of particulate aluminum in both the large (>51 µm) and small (1-51 µm) particles from USCGC Healy sampling is a better indicator of weak nepheloid layers (Xiang and Lam, 2020). They defined nepheloid layers as increases in particulate aluminum concentrations above 9 nM for small particles (1-51 µm) and 1 nM for large (>51 µm) particles. These nepheloid layers, especially those below 1000 m, are characterized by high lithogenic contents, 68.7 ± 8.7% (n=15) and 78.0 ± 7.9% (n=15) in the large size fraction and small size fraction, respectively. Nepheloid layer thickness based on particulate Al concentration varies from about 100 m to more than 1000 m for both size fractions. Xiang and Lam (2020) discuss several mechanisms that contribute to the transfer of sediment from the Arctic shelf to the deep basins. They speculated that density-driven shelf water cascading downslope during winter might be the major contributor to high lithogenic particles in the central Arctic Basin. Slightly stronger nepheloid layers were found in some isolated bathymetric lows in the northbound section through the Chukchi Borderland down into Makarov Basin (Figure 4) with PM concentrations of 3-10 µg l^{-1} (Xiang and Lam, 2020).

In nepheloid layers found in shallow basins (200-400 m) of the Barents Sea, Cp values were much higher than in the deep basins; an equivalent PM concentration of as much as ~200 µg l^{-1}, based on the shelf/slope PM and Cp relationship (Figure 2a). Nepheloid layers in this region are also most likely created when rapidly cooled water cascades down into the small basins, eroding and resuspending sediment.

Global measurements of PM concentration show a wide range of values in both

surface and near-bottom waters, but concentrations in the middle of the water column, i.e. between 200 m depth and a few hundred meters above the seafloor are generally less than about 5-12 µg l^{-1} (Brewer et al. 1976; Gardner et al., 2018a). Sufficient measurements have been made globally that we can map nepheloid layer characteristics such as maximum bottom concentration, integrated nepheloid layer mass and thickness (Gardner et al., 2018 a, b). One of the conclusions of that work was that nepheloid layers have the greatest intensity beneath areas of high eddy kinetic energy, which can occur below meanders of major boundary currents, e.g. Gulf Stream (Gardner et al., 2016). Given the seasonal ice cover of most of the Arctic Ocean, strong, wide, meandering boundary currents were not observed and are less likely than in ice-free waters.

6.2. Nepheloid layers along continental shelves and slopes in the Arctic Ocean.

Eddies play an important role in Arctic waters (Timmerman and Marshall, 2020; O'Brien et al., 2013) and satellite-derived eddy kinetic energy estimates show that shelf and shelf edge boundary current regions have higher energy than the interior Canada Basin and Nordic Seas (Armitage et al., 2017). As noted in section 4.2 (Figure 5), narrow, seasonally varying boundary currents with typical speeds around 15 cm s^{-1} (Timmerman and Marshall, 2020) are trapped at the shelf breaks in the Nansen, Canada and Makarov Basins. That speed is sufficient to resuspend sediments along the shelf and basin margins (Miller et al., 1977), but no currents close to that intensity have been reported in the deep basins. Thus, only minor sediment resuspension and weak nepheloid layers are observed near the seafloor in Arctic basins.

Depending on the wind strength, which is believed to drive the Slope Current, strong currents could be found down to at least 40 m to 125 m depth, but are not locked to a specific isobath and can meander laterally (Corlett and Pickart, 2017). Velocity estimates from their Figure 13 are about 20 cm s^{-1}, which is sufficient to resuspend bottom sediment. Some high concentrations of PM could move 50 - 300 km offshore based on our profiles, but high concentrations of particles do not appear to be carried deep into the Pacific halocline before settling out. Xiang and Lam (2020) find evidence of considerable lateral advection of lithogenic particles coming off the shelf. Timmermans and Marshall (2020) noted that there are also "narrow, energetic, seasonally varying boundary currents, with typical speeds around 15 cm s^{-1}, trapped at the shelf breaks" (see also Aksenov et al., 2011; Dmitrenko et al., 2016; Nikolopoulos et al., 2009; Pickart, 2004), which definitely could be missed given the USCGC Healy and R/V Polarstern 2015 expeditions' sampling patterns.

6.3. Role of Barrow Canyon on water and sediment dispersal.

Intermediate nepheloid layers with high PM concentrations are found in water bordering the Chukchi Sea between 100-600 m depth in both sections (Figures 3, 4). Timmerman and Marshall (2020) state that a major portion of the water coming through Bering Strait moves through or above Barrow Canyon. PM concentrations in water coming out of the Bering Strait are 2000 -4000 µg l^{-1} in

the bottom 30 m based on in-situ filtered pump samples, which are extremely high concentrations compared with the deep basins, but not unreasonable for active shelf areas. As noted in section 4.1, the Bering Strait water feeds the Alaska Coastal Current and moves off the Chukchi shelf before it splits into the Shelfbreak Current to the right (i.e. southeast) and the Slope Current to the left (i.e. northwest) (Figure 5) (Corlett and Pickart, 2017), so one might expect that the canyon should influence the hydro and sediment dynamics of the area as has been found in various canyons along the east coast of North America (Gardner, 1989; Hunkins, 1988; Puig et al. 2013). Many V-shaped canyons experience strong up-down canyon flows driven by tidal forcing that also resuspends sediment along the canyon axis during flow in both directions, carrying resuspended sediment down the canyon until it reaches water of an equivalent fluid density. At that point the sediment-laden water detaches from the seafloor and moves seaward along that density interface, with sediment settling out along the way. This has also been found along continental slopes (Cacchione and Drake, 1986) and could account for the high PM concentrations in water bordering the Chukchi Shelf in both sections (Figures 3 and 4). However, in contrast with currents reported in those North American east-coast canyons, currents measured in Barrow Canyon were less regular as discussed below.

In 1986-1987 Aagaard & Roach (1990) sought to measure hypersaline plumes in Barrow Canyon that were expected to occur during sea ice formation, but found none. Instead they found cold, relatively fresh water flowing downcanyon, temporally interspersed with warm, saline water flowing upcanyon as fast as 60 cm s^{-1}. They also found that flow was only weakly correlated with wind speed and atmospheric pressure gradients. However, they found coherence between upwelling events and flow reversals at sites 400 km apart along the coast, so they suggested that these events were caused by shelf waves propagating eastward along the Arctic Ocean margin. No measurements were made of PM in the water at that time, but the moored instruments attached well off the bottom released sediment-laden water during recovery through the sea-air interface –evidence that very turbid waters were common at near-bottom instrument depths and sediment accumulated on the instruments.

Mountain et al., (1976) measured currents for four months at 96 m and 126 m in 150 m water depth in Barrow Canyon. Currents were similar at both depths, moving along the axis, most often to the northeast (downcanyon), with occasional reversals to the southwest (upcanyon). Currents were similar at both depths with maximum velocities northeast up to 100 cm s^{-1} and short reversal periods southwest at 25 cm s^{-1}. It is unlikely that these currents persist very far down the canyon as they will encounter more dense water and will detach and spread out along a matching pycnocline. At the canyon depth of 143 m, currents most often moved up the canyon for periods that could last for weeks in the same direction (Mountain et al., 1976; Aagaard and Roach, 1990). Upcanyon speeds often reached more than 40 cm s^{-1} and sometimes 100 cm s^{-1}, though the long-term mean velocity was directed down canyon at 15 - 20 cm s^{-1}. The large changes in current speed and direction suggest that the intermediate nepheloid

layers observed along the Chukchi margin are not in steady state.

6.4 Evidence of PM transport from shelves to deep basins.

The strong currents coming through the Bering Strait and in Barrow canyon are obviously sufficient to resuspend and transport sediment as shown by the observed high Cp values (Figures 3, 4). Field studies using current meters, transmissometers, Chl-*a* fluorometers and sediment traps off of the Mackenzie shelf, ~500 km east of Barrow canyon, also showed occasional strong currents (100 cm s^{-1}) that resuspend carbon-rich shelf sediment and carry them out beyond the shelf into Canada Basin (Forest et al., 2007).

Honjo et al., (2010) found similar results in Canada Basin in a sediment trap experiment. They deployed a time-series sediment trap mooring at 3067 m in 3924 m of water (857 meters above the bottom) in the Canada Basin. Then they suspended time-series sediment traps from surface sea ice at two depths: 120 m and 200 m. The POC export flux registered by the surface trap was 2-3 orders of magnitude smaller than that measured at equivalent depths in lower latitude oceans, despite the fact that annual primary production was similar in both regions (Honjo et al., 2010). They attributed the difference to a poorly developed zooplankton ecosystem beneath the ice. Normally, zooplankton feed on phytoplankton and excrete fecal pellets that settle rapidly and drive the POC export. Beneath the ice in their study area, they noted the lack of diatom frustules, coccoliths and lithogenic particles that would add ballast to sinking fecal pellets or aggregates. As a result, they hypothesized that a large portion of the primary POC production in Canada Basin does not sink into the deep waters, but is remineralized in shallow waters. Analysis of the particles in the water column in 2015 shows a steady decline with depth in the fraction of particles that are organic matter and an increase in the percent of lithogenic particles (Xiang and Lam, 2020, their Figures 5 and 6). Opal and $CaCO_3$ are not abundant in the small particles, but opal consists of upwards of 60% of the large particles in surface waters, and could provide ballast to settling particles.

The mass flux measured in the bottom-moored trap (in 2004-2005) by Honjo et al. (2010) was an order of magnitude higher than recorded by the surface tethered traps (in 1996-1997). The POC flux was 4-50% higher in the deep traps and had much more lithogenic clay-sized particles (85%). Honjo et al., (2010) assumed that lithogenic material was moved off the shelf/slope margins and carried into the deep basin, forming a nepheloid layer. This is consistent with findings of Xiang and Lam (2020, their Figures 5 and 6) in that whereas biogenic particles (POC and opal) dominate the upper 1000 m, lithogenic particles are the most abundant particle type at greater depths. Hwang et al. (2015) deployed sediment traps at different depths in the southwestern part of the deep Canada Basin and reported slightly elevated particle flux and lower ^{14}C values at 3750 m than at 2000 m and 3000 m, implying the existence of a bottom nepheloid layer although weak. This also is consistent with the slightly higher concentration we measured near the seafloor in the deep basins.

Results of long-term sediment trap deployments in Canada Basin off the Mackenzie shelf confirmed off-shelf transport of sediment that decreased with distance from the shelf and was highly variable on an intra-annual time scale (O'Brien et al., 2013). They also noted the strong influence of cyclonic and anti-cyclonic eddies on sedimentation rates.

Our optical data (Figures 3 and 4) show a slightly higher particle concentration near the seafloor in the deep basins and some higher Cp values near the margins, but there are few areas beyond the shelf where bottom PM concentrations are significantly elevated based on Cp measurements. Particulate Al measured in filtered water samples shows the increase in near-bottom lithogenic concentrations more distinctly (Xiang and Lam, 2020). It is also possible that the fine-grained material swept off the shelf forms large aggregates during settling. The transmissometer beam attenuation signal comes mostly from particles 1 - 20 microns and is less sensitive to particles > 20 microns (Gardner et al., 1993; Boss et al 2009; Boss et al, 2015;), so larger aggregates could settle undetected, or under-detected, by transmissometers. However, in-situ pump sampling shows no evidence of abundant large aggregates.

7. Conclusions

The combination of Cp (a proxy for PM and POC) plotted with salinity, temperature and Chl-*a* adds a background and baseline across the entire Arctic Ocean that are important in understanding the dynamics of the Arctic. The high vertical and horizontal resolution of the particle distribution in the sections compiled here using optical data, paints a rich picture of particle distribution and sources. However, this is just a two-month snapshot in a single year and there are undoubtedly seasonal and spatial changes in addition to well-documented climatological changes, especially beneath ice-free areas. Changes in the deeper water column are far less likely because there is no outflow path from the deep basins.

Particle- and nutrient-rich water coming from the Pacific through Bering Strait sinks below the low-salinity, nutrient-poor PML. Ice pack limits the light available for photosynthesis in surface waters of the Beaufort Sea. Based on Chl-*a* and POC (from Cp) distribution, biomass from primary production was larger at time of sampling in the Barents Sea than in the Beaufort Sea, presumably because nutrient-rich water coming into the Barents Sea is not isolated from surface waters by strong stratification and sea ice. Subsurface Chl-a maxima were found along both transects and form when nutrient-rich waters (nitrate >0.5 µg l^{-1}) occur within the euphotic zone.

River-borne and shelf sediment can enter the Arctic basins by shelf currents, eddies, submarine canyon currents and internal wave/tide dynamics, but most of the fine sediment settles out within a few tens to a hundred km from the margins. Nutrients from pore waters of resuspended sediments can be carried seaward by similar processes, but possibly transported for a longer distance laterally, as evidenced by the presence of Ra-228 traced back to Chukchi shelf

and Siberian rivers.

Benthic nepheloid layers are weak in most Arctic basins, but they are manifest by very slight increases in Cp and a more distinct increase in particulate aluminum concentrations. However, currents are too weak in the deep basins to cause significant erosion and resuspension. Areas with significant topography such as the Chukchi Borderland and the shallower Barents Sea basins are more likely to have isolated benthic nepheloid layers due in part to cascading of dense water sinking during rapid cooling of surface waters.

Acknowledgements:

We thank the captains and crews of USCGC Healy and R/V Polarstern plus chief scientists Dave Kadko, Bill Landing, and all science personnel aboard the USCGC Healy and chief scientist Ursula Schauer and all science personnel on the R/V Polarstern for collecting data during the joint GEOTRACES 2015 Arctic expeditions. Supportive cooperation was provided by many personnel from the SIO Ocean Data Facility for USCGC Healy hydrographic data and by Benjamin Rabe from Alfred Wegener Institute for R/V Polarstern hydrographic data (PANGAEA datasets: Schauer (2016, http://doi.org/10.2312/BzPM_0703_2016), Rabe et al., (2016a, https://urldefense.com/v3/__https://doi.org/10.1594/PANGAEA.859559. 2016b, https://urldefense.com/v3/__https://doi.org/10.1594/PANGAEA.859558)). USCGC Healy transmissometer, fluorometer and hydrographic data are available through CCHDO expocode 33HQ20150809. All size-fractionated particle concentration and composition data described above are available on the Biological and Chemical Oceanography Data Management Office website (https://www.bco-dmo.org/dataset/807340). Carl Lamborg and Angelique White are thanked for collecting and analyzing the pigments using HPLC. We thank Reiner Schlitzer for development of Ocean Data View software that we use for data analyses and figure compilations. Two reviewers are thanked for their suggestions and questions that helped us improve the manuscript. Analysis and synthesis of these data has been supported by: US National Science Foundation (contract OCE-1536565 to Gardner and Richardson; OCE-1535854 to Lam), NOAA (grant NA19NES4320002 to Mishonov at Cooperative Institute for Satellite Earth System Studies -CISESS) at the University of Maryland/ESSIC and NCEI/NOAA (both US), and support from the TAMU Earl F. Cook Professorship (Gardner).

References cited

Aagaard, K. & Roach, A. T. (1990). Arctic Ocean-Shelf Exchange' Measurements in Barrow Canyon, *Journal of Geophysical Research, 95*:18,163 – 18,175.

Aksenov, Y., Ivanov, V. V., Nurser, A. G., Bacon, S., Polyakov, I. V., Coward, A. C., et al. (2011). The Arctic circumpolar boundary current. *Journal of Geophysical Research, 116*, C09017. https://doi.org/10.1029/2010JC006637.

Ardyna, M., Babin, M., Gosselin, M., Devred, E., Belanger, S., Matsuoka, A.,

& Tremblay, J.-E. (2013). Parameterization of vertical chlorophyll a in the Arctic Ocean: Impact of the subsurface chlorophyll maximum on regional, seasonal, and annual primary production estimates. *Biogeosciences, 10,* 4383–4404, doi:10.5194/bg-10-4383-2013.

Armitage, T. W. K., Bacon, S., Ridout, A. L., Petty, A. A., Wolbach, S., & Tsamados, M. (2017). Arctic Ocean geostrophic circulation 2003-2014. *The Cryosphere Discussions,* 2017, 1–32.

Baker, E. T., & Lavelle, J. W. (1984). The effect of particle size on the light attenuation coefficient of natural suspensions. *Journal of Geophysical Research 89*, 8197-8203.

Behrenfeld, M.J. & Boss, E. (2006). Beam attenuation and chlorophyll concentration as alternative optical indices of phytoplankton biomass. *Journal of Marine Research, 64,*431-451.

Bidigare, R.R., Van Heukelem, L., & Trees, C.C., (2005). Analysis of algal pigments by high-performance liquid chromatography, In: Andersen, R.A. (ed.), Algal Culturing Techniques. Academic Press, New York, New York, pp. 327-345.

Bishop, J.K.B., & Wood, T.J., (2008). Particulate matter chemistry and dynamics in the twilight zone at VERTIGO ALOHA and K2 sites. *Deep Sea Research Part I*: 55, 1684-1706.

Boss, E., Slade, W.H., Behrenfeld, M., & Dall'Olmo, G. (2009). Acceptance angle effects on the beam attenuation in the ocean. *Optics Express, 17,* 1535-1550.

Boss, E., Guidi, L., Richardson, M.J., Stemmann, L., Gardner, W., Bishop, J.K.B., Anderson, R.F., & Sherrell, R.M. (2015). Optical techniques for remote and in-situ characterization of particles pertinent to GEOTRACES. *Progress in Oceanography, 133*, 43-54. doi: http://dx.doi.org/10.1016/j.pocean.2014.09.007.

Brewer, P.G., Spencer, D.W., Biscaye, P.E., Hanley, A., Sachs, P.S., Smith, C.L., Kadar, S., & Fredericks, J. (1976). The distribution of particulate matter in the Atlantic Ocean. *Earth Planetary Science Letters, 32,* 393–402.

Cacchione, D. A. & Drake, D. E. (1986). Nepheloid layers and internal waves over continental shelves and slopes. *Geo-Marine Letters*, 6, 147-152. 10.1007/BF02238085.

Charette, M.A., Kipp, L. E., Jensen, L. T., Dabrowski, J. S., Whitmore, L. M., Fitzsimmons, J. N., et al. (2020). The Transpolar Drift as a source of riverine and shelf-derived trace elements to the central Arctic Ocean. *Journal of Geophysical Research, Oceans, 125*, (5), 1-34. DOI: 10.1029/2019JC015920.

Corlett, W.B. & Pickart, R.S. (2017). The Chukchi slope current. *Progress in Oceanography, 153*, 50–65.

Coupel, P., D. Ruiz-Pino, D., Sicre, M. A., Chen, J. F., Lee, S. H., Schiffrine, N., Li, H. L., & Gascard, J. C. (2015). The impact of freshening on phytoplankton production in the Pacific Arctic Ocean. *Progress in Oceanography*, 131: 113–125. doi:10.1016/ j.pocean.2014.12.003.

Desortová, B. (1981). Relationship between Chlorophyll- Concentration and Phytoplankton Biomass in Several Reservoirs in Czechoslovakia. *Hydrobiology,* 66, 153-169. https://doi.org/10.1002/iroh.19810660202.

Dmitrenko, I. A., Kirillov, S. A., Forest, A., Gratton, Y., Volkov, D. L., Williams, W. J., Lukovich, J. V., Belanger, C., & Barber, D.G. (2016). Shelf-break current over the Canadian Beaufort Sea continental slope: Wind-driven events in January 2005. *Journal of Geophysical Research: Oceans, 12*1, 2447–2468. https://doi.org/10.1002/2015JC011514.

Fetterer, F., K. Knowles, W. N. Meier, M. Savoie, & A. K. Windnagel. 2017, updated daily. Sea Ice Index, Version 3. Boulder, Colorado USA. NSIDC: National Snow and Ice Data Center. doi: https://doi.org/10.7265/N5K072F8.

Forest, A., Sampei, M., Hattori, H., Makabe, R., Sasaki, H., Fukuchi, M., Wassmann, P., & Fortier, L. (2007). Particulate organic carbon fluxes on the slope of the Mackenzie Shelf (Beaufort Sea): Physical and biological forcing of shelf-basin exchanges. *Journal of Marine Systems, 68,* 39– 54, doi:10.1016/ j.jmarsys.2006.10.008.

Gardner, W. D. (1989). Periodic resuspension in Baltimore Canyon by focusing of internal waves. *Journal of Geophysical Research, 94,* 18185-18194.

Gardner, W. D., Biscaye, P. E., Zaneveld, J. R. V., & Richardson, M. J. (1985). Calibration and comparison of the LDGO nephelometer and the OSU transmissometer on the Nova Scotian Rise. *Marine Geology 66*, 323-344.

Gardner, W.D., Tucholke, B.E., Richardson, M.J., & Biscaye, P.E. (2016). Benthic storms, nepheloid layers, and linkage with upper ocean dynamics in the Western North Atlantic. *Marine Geology*, http://dx.doi.org/10.1016/j.margeo.2016.12.012.

Gardner, W.D., Richardson, M.J., & Mishonov, A.V. (2018a). Global assessment of benthic nepheloid layers and linkage with upper ocean dynamics. *Earth and Planetary Science Letters, 482*, 126–134, https://doi.org/10.1016/j.epsl.2017.11.008.

Gardner, W.D., Richardson, M.J., Mishonov, A.V., & Biscaye, P.E. (2018b). Global comparison of Benthic Nepheloid Layers Based on 52 years of Nephelometer and Transmissometer Measurements. *Progress in Oceanography, 168,* 100-111. https://doi.org/10.1016/j.pocean.2018.09.008

Gardner, W.D., Walsh, I.D., & Richardson, M.J. (1993). Biophysical forcing of particle production and distribution during a spring bloom in the North Atlantic. *Deep Sea Research Part II: Topical Studies in Oceanography, 40,* 171–195.

Hedges, J., Baldock, J., Gélinas, Y., Lee, C., Peterson, M., & Wakeham, S., 2002. The biochemical and elemental compositions of marine plankton: A NMR perspective. *Marine Chemistry*, 78, 47-63. doi: 10.1016/S0304-4203(02)00009-9.

Honjo, S., Richard A. Krishfield, R. A., Eglinton, T.I., Manganini, S.J., Kempa, J. N., Doherty, K., Hwang, J., McKee, T. K., & Takizawa, T. (2010). Biological pump processes in the cryopelagic and hemipelagic Arctic Ocean: Canada Basin and Chukchi Rise. *Progress in Oceanography, 85,* 137-170.

Hunkins, K. P., Thorndike, E. M., & Mathieu, G. (1969). Nepheloid layers and bottom currents in the Arctic ocean. *Journal of Geophysical Research*, *74*, 6995-7008.

Hunkins, K. (1988)., Mean and tidal currents in Baltimore Canyon, *Journal of Geophysical Research.*, *93*, 6917-6929.

Hwang, J., M. Kim, S. J. Manganini, C. P. McIntyre, N. Haghipour, J.J. Park, R. A. Krishfield, R. W. Macdonald, F. A. McLaughlin, & T. I. Eglinton (2015). Temporal and spatial variability of particle transport in the deep Arctic Canada Basin, *Journal of Geophysical Research.* Oceans, 120, 2784–2799, doi:10.1002/2014JC010643.

Ivanov, V.V., Shapiro, G. I., Huthnance, J.M, Aleynik, D. L., & Golovin, P. N. (2004). Cascades of dense water around the world ocean. *Progress in Oceanography 60*, 47–98.

Jakobsen, H.H. & Markager, S. (2016). Carbon-to-chlorophyll ratio for phytoplankton in temperate coastal waters: Seasonal patterns and relationship to nutrients. *Limnology and Oceanogrphy, 61,* 1853-1868.

Jackson, J.M., Allen, S. E., Carmack, E. C., & McLaughlin, F. A. (2010). Suspended particles in the Canada Basin from optical and bottle data, 2003–2008. *Ocean Science 6,* 799–813.

Jensen, L. T., Morton, P., Twining, B. S., Heller, M. I., Hatta, M., Measures, C. I., John, S. G., Zhang, R., Pinedo-Gonzalez, P., Sherrell, R. M., & Fitzsimmons, J. N. (2020). A comparison of marine Fe and Mn cycling: U.S. GEOTRACES GN01 Western Arctic case study. *Geochimica et Cosmochimica Acta 288,* 138-160. doi: 1016/j.gca.2020.08.006.

Jones, E. P. (2001). Circulation in the Arctic ocean. *Polar Research*, *20*(2), 139-146.

Jones, E. P., Swift, J. H., Anderson, L. G., Lipozer, M., Civitarese, G., Falkner, K. K., Katner, G., & McLaughlin, F. (2003). Tracing Pacific water in the North Atlantic. *Journal of Geophysical Research, 108* (C4), 3116. doi:10.1029/2001JC001141.

Kadko, D. (2016). Cruise Report of the 2015 ARC01 US GEOTRACE/GO-SHIP.

Kadko, D., & Landing, W. (2015). U.S. Arctic GEOTRACES USCGC Healy (HLY1502) cruise report. Retrieved from https://www.bodc.ac.uk /resources/inventories/cruise_inventory/reports/healy1502.pdf.

Kadko, D., Pickart, R. S., & Mathis, J. (2008). Age characteristics of a shelf-break eddy in the western Arctic and implications for shelf-basin exchange. *Journal of Geophysical Research*, 113, C02018. https://doi.org/10.1029/2007JC004429.

Kipp, L. E., Kadko, D. C., Pickart, R. S., Henderson, P. B., Moore, W. S., & Charette, M. A. (2019). Shelf-basin interactions and water mass residence times in the Western Arctic Ocean: insights provided by radium isotopes. *Journal of Geophysical Research: Oceans, 124,* https://doi.org/10.1029/2019JC014988.

Kipp, L. E., Spall, M. A., Pickart, R. S., Kadko, D. C., Moore, W. S., Dabrowski, J. S., & Charette, M. A. (2020). Observational and modeling evidence of seasonal trends in sediment-derived material inputs to the Chukchi Sea. *Journal of Geophysical Research: Oceans,* 125, e2019JC016007. https:// doi.org/10.1029/2019JC016007.

Lam, P. J., Lee, J.-M., Heller, M. I., Mehic, S., Xiang, Y., & Bates, N. R. (2018). Size-fractionated distributions of suspended particle concentration and major phase composition from the U.S. GEOTRACES Eastern Pacific Zonal Transect (GP16). *Marine Chemistry, 201,* 90-107. https://doi.org/10.1016/j.marchem.2017.08.013.

Lam, P. J., Ohnemus, D.C., & Auro, M.E. (2015a). Size-fractionated major particle composition and concentrations from the US GEOTRACES North Atlantic Zonal Transect. *Deep Sea Research Part II: Topical Studies in Oceanography 116,* 303-320. http://dx.doi.org/10.1016/j.dsr2.2014.11.020.

Lam, P. J., Twining, B. S., Jeandel, C., Roychoudhury, A. N., Resing, J. A., Santschi, P. H., & Anderson, R. F. (2015b). Methods for analyzing the concentration and speciation of major and trace elements in marine particles. *Progress in Oceanography (special issue on particles), 133(0):* 32-42. doi:10.1016/j.pocean.2015.01.005.

Landry, M. R., Brown, S. L., Campbell, L., Constantinou, J., & Lui, H. (1998). "Spatial patterns in phytoplankton growth and microzooplankton grazing in the Arabian Sea during monsoon forcing." *Deep-Sea Research Part II: Topical Studies in Oceanography 45,* 2353-2368.

Lee, Z. P., Weidemann, A., Kindle, J. Arnone, R. Carder, K. L., & Davis, C. (2007). Euphotic zone depth: Its derivation and implication to ocean-color remote sensing. *Journal of Geophysical Research: Oceans*, 112, https://doi.or g/10.1029/2006JC003802.

Lorbacher K., Dommenget D., Niiler, P. P., & Köhl, A. (2006). Ocean mixed layer depth: A subsurface proxy of ocean-atmosphere variability. *Journal of Geophysical Research-Oceans*, 111, C7. https://doi.org/10.1029/2003JC002157.

Mathis, J. T., Pickart, R. S., Hansell, D. A., Kadko, D., & Bates, N. R. (2007). Eddy transport of organic carbon and nutrients from the Chukchi Shelf: Impact on the upper halocline of the western Arctic Ocean. *Journal of Geophysical Research*, 112, C05011. https://doi. org/10.1029/2006JC003899.

Miller, M. C., McCave, I. N., & Komar, P. D. (1977). Threshold of sediment motion under unidirectional currents. *Sedimentology*, *24*, 507-527.

Mishonov, A. V., Gardner, W. D., & Richardson, M. J. (2003). Remote sensing and surface POC concentration in the South Atlantic. *Deep Sea Research II*, *50* (22-26), p. 2997-3015. https://doi.org/10.1016/j.dsr2.2003.07.007.

Mountain, D. G., Coachman, L. K., & Aagaard, K. (1976). On the flow through Barrow Canyon. *Journal of Physical Oceanography, 6*, 461-470.

Nelson, C. D. & Creager, J. S. (1977). Displacement of Yukon-derived sediment from Bering Sea to Chukchi Sea during Holocene time. *Geology, 5* 141-146.

Nikolopoulos, A., Pickart, R. S., Fratantoni, P. S., Shimada, K., Torres, D. J., & Jones, E. P. (2009). The western Arctic boundary current at 152W: Structure, variability, and transport. *Deep Sea Research Part II: Topical Studies in Oceanography, 56(17),* 1164–1181.

Ober, S. Rijkenberg, M. & Gerringa, L. (2016a). Physical oceanography measured with ultra clean CTD/Water sampler-system during POLARSTERN cruise PS94 (ARK-XXIX/3) https://www.tib.eu/de/suchen/id/datacite: doi~10.1594%252FPANGAEA.859560/.

Ober, S. Rijkenberg, M. & Gerringa, L. (2016b). Physical oceanography measured on water bottle samples with ultra clean CTD/Water sampler-system during POLARSTERN cruise PS94 (ARK-XXIX/3) https://www.tib.eu/de/suchen/id/datacite:doi~10.1594%252FPANGAEA.859561.

O'Brien, M. C., Melling, H., Pedersen, T. F., & Macdonald, R. W. (2013). The role of eddies on particle flux in the Canada Basin of the Arctic Ocean. *Deep Sea Research Part I: Oceanographic Research Papers*, *71*, 1-20. doi:10.1016/j.dsr.2012.10.004.

Ohnemus, D. C., Lam, P. J., & Twining, B. S. (2018). Optical observation of particles and responses to particle composition in the GEOTRACES GP16 section. *Marine Chemistry 201,* 124-136. https://doi.org/10.1016/j.marchem.2017.09.004.

PANGAEA datasets:

> http://doi.org/10.2312/BzPM_0703_2016 and http://hdl.handle.net/10013/epic.48723.

Peralta-Ferriz, C., & Woodgate, R. A. (2015). Seasonal and interannual variability of pan-arctic surface mixed layer properties from 1979 to 2012 from hydrographic data, and the dominance of stratification for multiyear mixed layer depth shoaling. *Progress in Oceanography, 134,* 19–53.

Perovich, D., Meier, W., Tschudi, M., Farrell, S., Hendricks, S., Gerland, S., et al. (2019). Sea ice cover. In "State of the Climate in 2018". *Bulletin of the American Meteorological Society, 100(9),* S146–S150.

Pickart, R. S. (2004). Shelfbreak circulation in the Alaskan Beaufort Sea: Mean structure and variability. *Journal of Geophysical Research, 109,* C04024. https://doi.org/10.1029/2003JC001912.

Pickart, R. S., Weingartner, T. J., Pratt, L. J., Zimmermann, S. & Torres, D. J. (2005). Flow of winter-transformed Pacific water into the Western Arctic. *Deep Sea Research, II Topical Studies in Oceanography.* 52, 3175–3198. https://doi.org/10.1016/j.dsr2.2005.10.009.

Puig, P., Greenan, B. J. W., Li, M. Z., Prescott, R. H., & Piper, D. J. W. (2013). Sediment transport processes at the head of Halibut Canyon, Eastern Canada margin: An interplay between internal tides and dense shelf-water cascading. *Marine Geology 341*, 14–28.

Rabe, B., Schauer, U., Ober, S., Horn, M., Hoppmann, M., Korhonen, M., Pisarev, S., Hampe, H., Villacieros, N., Savy, J. P., & Wisotzki, A. (2016a): Physical oceanography measured on water bottle samples during POLARSTERN cruise PS94 (ARK-XXIX/3). Alfred Wegener Institute, Helmholtz Centre for Polar and Marine Research, Bremerhaven, PANGAEA, https://urldefense.com/v3/___https://doi.org/10.1594/PANGAEA.859559.

Rabe, B., Schauer, U., Ober, S., Horn, M., Hoppmann, M., Korhonen, M., Pisarev, S., Hampe, H., Villacieros, N., Savy, J. P., & Wisotzki, A. (2016b): Physical oceanography during POLARSTERN cruise PS94 (ARK-XXIX/3). Alfred Wegener Institute, Helmholtz Centre for Polar and Marine Research, Bremerhaven, PANGAEA, https://urldefense.com/v3/___https://doi.org/10.1594/PANGAEA.859558.

Roach, A. T., Aagaard, K., Pease, C. H., Salo, S. A., Weingartner, T., Pavlov, V., & Kulakov, M. (1995). Direct measurement of transport and water properties through the Bering Strait. *Journal of Geophysical Research, 100 (C9),* 18443–18457.

Roesler, C., Uitz, J., Claustre, H., Boss, E., Xing, X., Organelli, E., Briggs, E., Bricaud, A., Schmechtig, C. Poteau, A., D'Ortenzio, F., Ras, J., Drapeau, S., Haentjens, N., & Barbieux, M. (2017). Recommendations for obtaining unbiased chlorophyll estimates from in situ chlorophyll fluorometers: A global analysis of WET Labs ECO sensors. *Limnology and Oceanography: Methods* 15, 2017, 572–585, doi: 10.1002/lom3.10185.

Rudels, B., Jones, E. P., Schauer, U., & Eriksson, P. (2004). Atlantic sources of the Arctic Ocean surface and halocline waters. *Polar Research, 23(2),* 181–208. https://doi.org/10.3402/polar.v23i2.6278.

Rutgers van der Loeff, M., Kipp, L., Charette, M. A., Moore, W. S., Black, E., Stimac, I., et al. (2018). Radium isotopes across the Arctic Ocean show time scales of water mass ventilation and increasing shelf inputs. *Journal of*

Geophysical Research: Oceans, 123, 4853–4873. https://doi.org/10.1029/2018JC013888.

Schauer, U., The Expedition PS94 of the Research Vessel POLARSTERN to the central Arctic Ocean in 2015 (2016). Reports on polar and marine research, Bremerhaven, Alfred Wegener Institute for Polar and Marine Research, 703, 170 p. http://doi.org/10.2312/BzPM_0703_2016.

Schlitzer, R. (2020). Ocean Data View, https://odv.awi.de.

Seidov, D., Antonov, J. I., Arzayus, K. M., Baranova, O. K., Biddle, M., Boyer, T. P., Johnson, D. R., Mishonov, A. V., Paver, C., & Zweng M. M. (2015). Oceanography north of 60°N from World Ocean Database. *Progress in Oceanography, 132*, 153-173, ISSN 0079-6611, https://doi.org/10.1016/j.pocean.2014.02.003.

Slagter, H. A., Reader, H. E., Rijkenberg, M. J. A., Rutgers van der Loeff, M., Baar, H. J. W. D., & Gerringa, L. J. A. (2017). Organic Fe speciation in the Eurasian Basins of the Arctic Ocean and its relation to terrestrial DOM. *Marine Chemistry, 197,* 11–25.

Spall, M., Pickart, R., Li, M., Itoh, M., Lin, P., Kikuchi, T., & Qi, Y. (2018). Transport of Pacific water into the Canada Basin and the formation of the Chukchi Slope Current. Journal of Geophysical Research: Oceans, 123, 7453–7471. https://doi.org/10.1029/2018JC013825.

Steele, M., Morison, J., Ermold, W., Rigor, I., Ortmeyer, M., & Shimada, K. (2004). Circulation of summer pacific halocline water in the arctic ocean. *Journal of Geophysical Research: Oceans, 109,* C02027. http://dx.doi.org/10.1029/2003JC002009.

Steiner, N., Sou, T., Deal, C., Jackson, J. M., Jin, M., Popova, E., Williams, W., & Yool, A. (2016). The Future of the Subsurface Chlorophyll-a Maximum in the Canada Basin - A Model Intercomparison, *Journal of Geophysical Research Oceans, 121(1),* 387-409, DOI:10.1002/2015JC011232.

Strom, S.L. (1993). Production of pheopigments by marine protozoa: results of laboratory experiments analysed by HPLC, *Deep Sea Research Part I, 40*, 57-80. https://doi.org/10.1016/0967-0637(93)90053-6.

Thorndike, E., & Ewing, M. (1967). Photographic nephelometers for the deep sea, Chap. 10, in Deep-Sea Photography, edited by J. B. Hersey, Johns Hopkins Press, pp. 113-116, Baltimore, Md., 1967.

Timmermans, M.-L., & Marshall, J. (2020). Understanding Arctic Ocean circulation: A review of ocean dynamics in a changing climate. *Journal of Geophysical Research: Oceans, 125,* e2018JC014378. https://doi.org/10.1029/2018JC014378.

Toole, J. M., Timmermans, M.-L., Perovich, D. K., Krishfield, R. A., Proshutinsky, A., & Richter-Menge, J. A. (2010). Influences of the ocean surface mixed layer and thermohaline stratification on Arctic sea ice in the central Canada

Basin. *Journal of Geophysical Research, 115,* C10018. https://doi.org/10.1029/2009JC005660.

Watanabe, E., Onodera, J., Harada, N., Honda, M. C., Kimoto, K., Kikuchi, T., Nishino, S., Matsuno, K., Yamaguchi, A., Ishida, A. & Kishi, M. J. (2014). Enhanced role of eddies in the Arctic marine biological pump. Nature Communications 5. https://doi.org/10.1038/ncomms4950.

Xiang, Y., & Lam, P. J. (2020). Size-fractionated compositions of marine suspended particles in the western Arctic Ocean: Lateral and vertical sources. *Journal of Geophysical Research: Oceans*, 125, e2020JC016144. https://doi.org/10.1029/2020JC016144.